Electronic Supplementary Material (ESI) for Physical Chemistry Chemical Physics.

Supplementary information for:

On the elusive nature of Oxygen binding at coordinatively unsaturated 3d transition metal centers in metal-organic frameworks

Mali H. Rosnes[a], D. Sheptyakov[b], A. Franz[c], M. Frontzek[d], Pascal D. C. Dietzel[a*], P. A. Georgiev[e,f*],

[a]Department of Chemistry, University of Bergen, P.O. Box 7803, N-5020 Bergen, Norway.
[b]Laboratory for NeutronScattering, Paul Scherrer Institut, CH-5232 Villigen, Switzerland
[c]Helmholtz-Zentrum Berlin für Materialien und Energie GmbHHahn-Meitner-Platz 114109 Berlin
[d]Quantum Condensed Matter Division, Oak Ridge National Laboratory, 37831 Oak Ridge, TN, USA
[e]Department of Chemistry, University of Milan, 21 Via Golgi, I-20133 Milan, Italy.
[f]Faculty of Physics, University of Sofia, James Bourchier 5, 1164 Sofia, Bulgaria

Materials

All chemicals, reagents and solvents were purchased from Sigma-Aldrich and used as received without further purification. CPO-27-M were all synthesised under solvothermal conditions, and processed under inert conditions. The gases used for gas adsorption measurements were of 99.999%, or higher, purity and were purchased from Yara Praxair.

Preparation of [Mn(C_4HO_3)] (CPO-27-Mn). *2*,5-dihydroxyterephthalic acid (0.743 g, 3.75 mmol) was dissolved in N-methyl-2-pyrrolidone (50 mL) in a Teflon-lined insert (125 mL volume). A solution of manganese(II) acetate tetrahydrate (1.838 g, 7.5 mmol) in H_2O (6 mL) was added, and the insert was placed in an autoclave, sealed and reacted for 24 h at 110 °C in a preheated furnace. Filtration in a Schlenk apparatus yielded orange-red material and a little amount of colourless precipitate. The material was washed with copious amounts of water during which the main component changed its colour to orange and the colourless substance dissolved and washed away. The supernatant solvent was replaced by methanol three times, leaving each portion to stand for about 30 min, before it was filtered in a Schlenk apparatus. Finally, the product was dried at 150 °C in dynamic vacuum. Yield [Mn(C_4HO_3)] (151.99 g mol^{-1}): 0.444 g (38.9 %). Powder X-ray diffraction confirms the identity of the compound. Accessibility of the void volume was confirmed by nitrogen gas adsorption: BET surface area of 1264 $m^2\ g^{-1}$, Langmuir surface area of 1676 $m^2\ g^{-1}$ and total pore volume (at p / p_0 = 0.500) of 0.58 $cm^3\ g^{-1}$.

Preparation of [Co(C_4HO_3)] (CPO-27-Co). 2,5-dihydroxyterephthalic acid (1.981 g, 10 mmol) was dissolved in THF (30 mL) in a Teflon-lined insert (125 mL volume). A solution of cobalt(II) acetate tetrahydrate (4.982 g, 20 mmol) in H_2O (30 mL) was added, and the insert was placed in an autoclave, sealed and reacted for 24 h at 110 °C in a preheated furnace. The material was washed with H_2O before the supernatant solvent was replaced by methanol three times, leaving each portion to stand for about 30 min, before it was filtered in a Schlenk apparatus. Finally, the product was dried at 150 °C in dynamic vacuum. Yield [Co(C_4HO_3)] (155.98 g mol^{-1}): 2.542 g (81.5 %). Powder X-ray diffraction confirms the identity of the compound. Accessibility of the void volume was confirmed by nitrogen gas adsorption: BET surface area of 1276 $m^2\ g^{-1}$, Langmuir surface area of 1362 $m^2\ g^{-1}$ and total pore volume (at p / p_0 = 0.500) of 0.48 $cm^3\ g^{-1}$.

Preparation of [Ni(C_4HO_3)] (CPO-27-Ni). A solution of nickel(II) acetate tetrahydrate (4.977 g, 20 mmol) and 2,5-dihydroxyterephthalic acid (1.981 g, 10 mmol) was dissolved in H_2O (60 mL) in a Teflon-lined insert (125 mL volume). The insert was placed in an autoclave, sealed and reacted for 24 h at 110 °C in a preheated furnace. Filtration under inert conditions resulted in a yellow crystalline material consisting of very crystalline material. The material was washed with H_2O before the supernatant solvent was replaced by methanol three times, leaving each portion to stand for about 30 min, before it was filtered in a Schlenk apparatus. Finally, the product was dried at 150 °C in dynamic vacuum. Yield [Ni(C_4HO_3)] (155.74 g mol^{-1}): 2.379 g (76.4 %). Powder X-ray diffraction confirms the identity of the compound. Accessibility of the void volume was confirmed by nitrogen gas adsorption: BET surface area of 1107 $m^2\ g^{-1}$, Langmuir surface area of 1234 $m^2\ g^{-1}$ and total pore volume (at p / p_0 = 0.500) of 0.43 $cm^3\ g^{-1}$.

Preparation of [Cu(C_4HO_3)] (CPO-27-Cu). A mixture of 2,5-dihydroxyterephthalic acid (0.991 g, 5.0 mmol), 1,4-diazabicyclo[2.2.2]octane (DABCO, 0.280 g, 2.5 mmol) and copper(II) nitrate hemi(pentahydrate) (2.326 g, 10.0 mmol) in *N*,*N*-dimethylformamide (DMF, 65 mL) was stirred for 10 min in a Teflon-lined insert (125

mL volume). The insert was placed in an autoclave, sealed and reacted for 3 days at 60 °C in a preheated furnace. Filtration under inert conditions resulted in a very dark reddish-brown crystalline material consisting of very fine needle shaped crystals. The material was washed with DMF before the supernatant solvent was replaced by methanol three times, leaving each portion to stand for about 30 min, before it was filtered in a Schlenk apparatus. Finally the product was dried at 120 °C in dynamic vacuum. Yield [Cu(C_4HO_3)] (160.59 g mol^{-1}): 0.550 g (68 %). Powder X-ray diffraction confirms the identity of the compound. Accessibility of the void volume was confirmed by nitrogen gas adsorption: BET surface area of 1251 m^2 g^{-1}, Langmuir surface area of 1346 m^2 g^{-1} and total pore volume (at p / p_0 = 0.500) of 0.47 cm^3 g^{-1}.

Preparation of [Zn(C_4HO_3)] (CPO-27-Zn). 2,5-dihydroxyterephthalic acid (0.495 g, 2.5 mmol) was dissolved in THF (30 mL) in a Teflon-lined insert (125 mL volume). After five minutes an aqueous solution of sodium hydroxide (1.0 mol L^{-1}, 0.0097 g, 10 mmol) was added to the insert and stirred for five minutes before a solution of zinc(II) nitrate hexahydrate (1.487 g, 5.0 mmol) in H_2O (10 mL) were added. The insert was placed in an autoclave, sealed and reacted for 24 h at 120 °C in a preheated furnace. The material was washed with copious amounts of H_2O during which the main component changed its colour to orange and the colourless substance dissolved and washed away. The supernatant solvent was replaced by methanol three times, leaving each portion to stand for about 30 min, before it was filtered in a Schlenk apparatus. Finally, the product was dried at 150 °C in dynamic vacuum. Yield [Zn(C_4HO_3)] (162.44 g mol^{-1}): 0.630 g (77.6 %). Powder X-ray diffraction confirms the identity of the compound. Accessibility of the void volume was confirmed by nitrogen gas adsorption: BET surface area of 1187 m^2 g^{-1}, Langmuir surface area of 1274 m^2 g^{-1} and total pore volume (at p / p_0 = 0.500) of 0.45 cm^3 g^{-1}.

Sorption Measurements

For the Q_{st} calculations, the adsorption data was fitted using the single-site Langmuir-Freundlich equation.[9,16,17]

Equation 1. Single-site Langmuir-Freundlich model.

$$n_{ads} = \frac{n_{sat,1} b_1 P_1^{v_1}}{1 + b_1 P_1^{v_1}}$$

Equation 2. The single-site Langmuir-Freundlich model rearranged for *P*.

$$P_1 = \left(\frac{n_{ads}}{n_{sat,1} b_1 - n_{ads} b_1} \right)^{\frac{1}{v_1}}$$

Table S1. An overview of the parameters used in equations 1 and 2.

Parameter	Definition
n_{ads}	Molar loading of adsorbate, mol g^{-1}
$n_{sat,1}$	Saturation loading, mol g^{-1}
b_1	Parameter in the pure component Langmuir adsorption isotherm, kPa^{-1}
p_1	Bulk gas phase pressure, kPa
v_1	Exponent in the single-site Langmuir-Freundlich isotherm, dimensionless

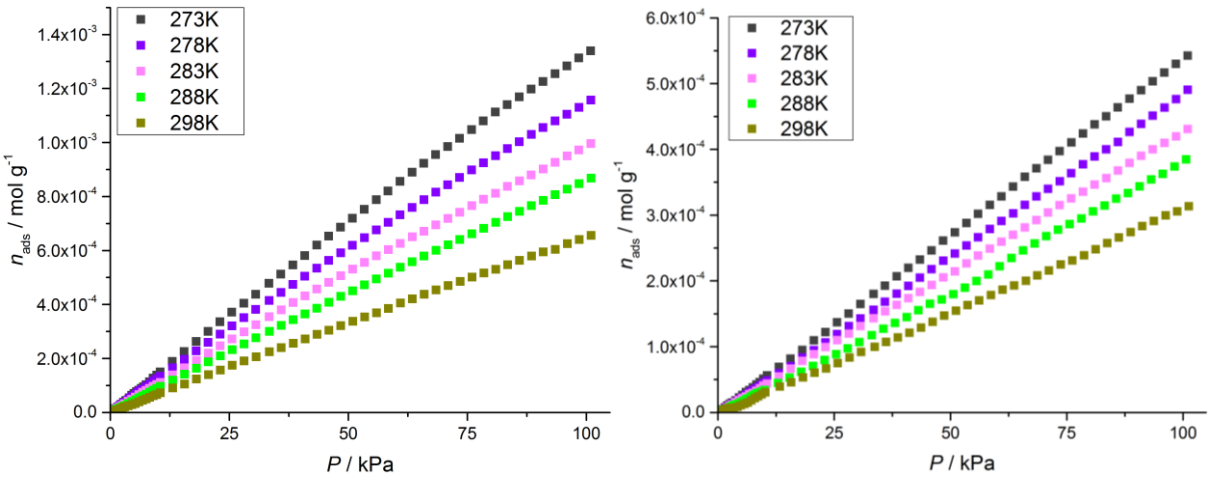

Figure S1. N_2 (left) and O_2 (right) adsorption in CPO-27-Co at room temperature.

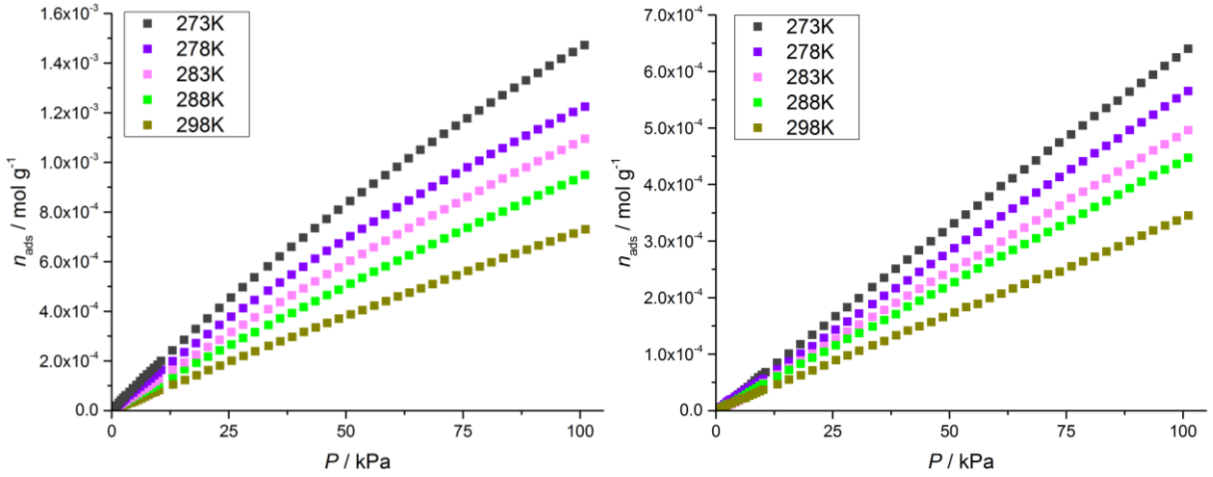

Figure S2. N_2 (left) and O_2 (right) adsorption in CPO-27-Ni at room temperature.

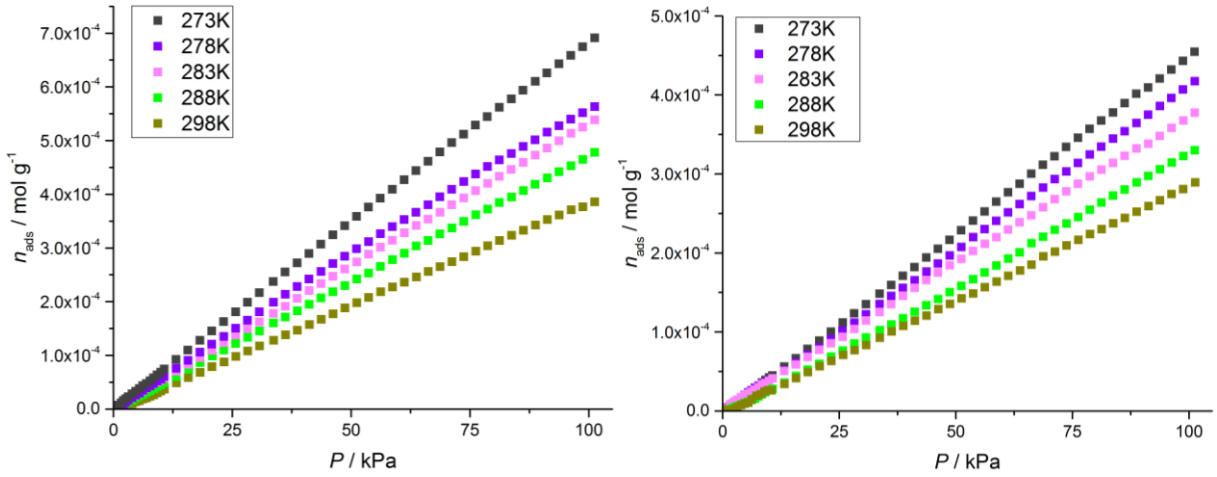

Figure S3. N_2 (left) and O_2 (right) adsorption in CPO-27-Mn at room temperature.

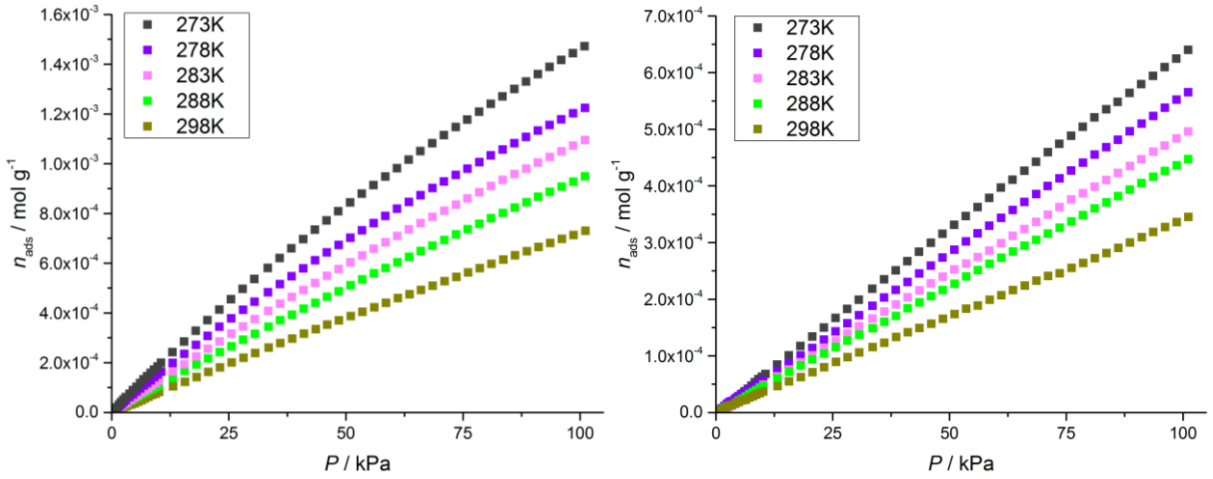

Figure S4. N_2 (left) and O_2 (right) adsorption in CPO-27-Cu at room temperature.

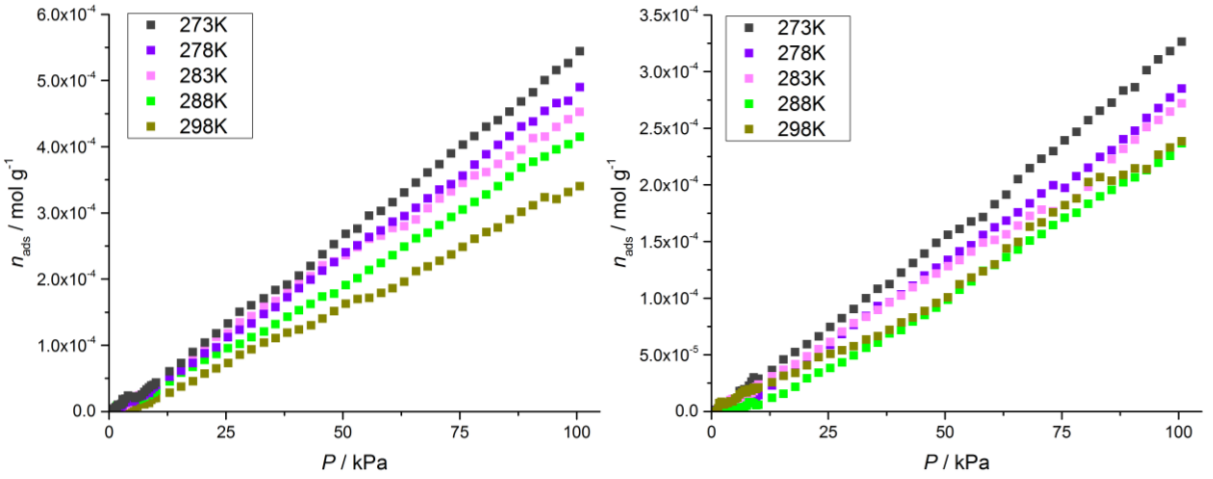

Figure S5. N_2 (left) and O_2 (right) adsorption in CPO-27-Zn at room temperature.

Langmuir-Freundlich fits of CPO-27-Co with nitrogen:

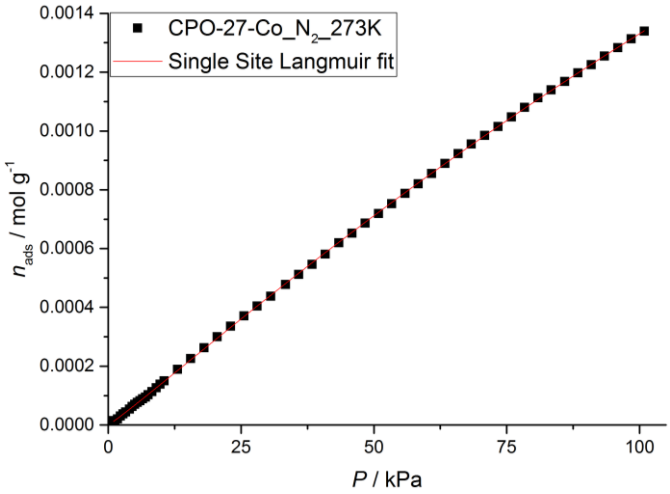

Figure S6. The single-site Langmuir-Freundlich fit for nitrogen in CPO-27-Co at 273 K.

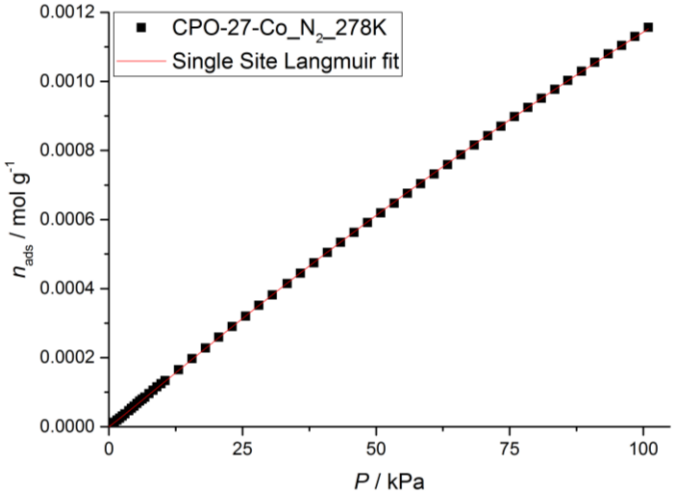

Figure S7. The single-site Langmuir-Freundlich fit for nitrogen in CPO-27-Co at 278 K.

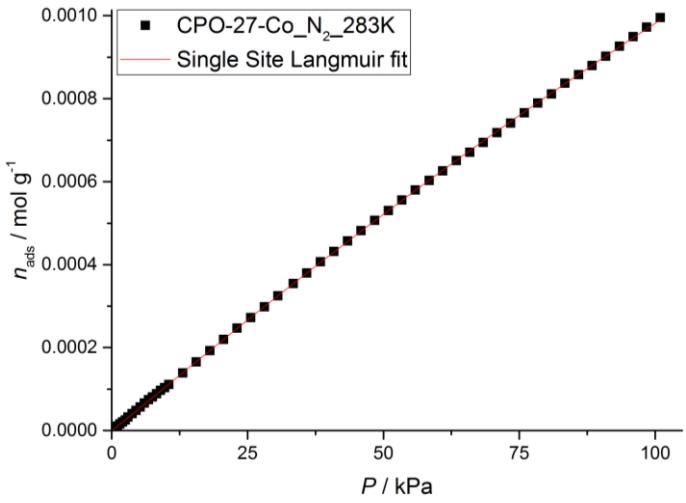

Figure S8. The single-site Langmuir-Freundlich fit for nitrogen in CPO-27-Co at 283 K.

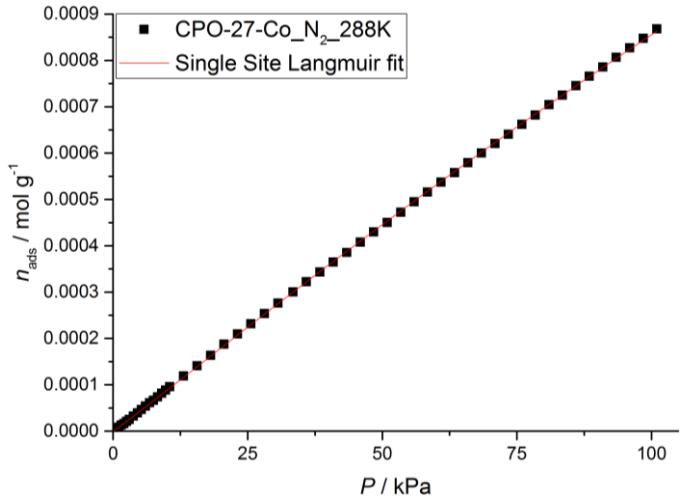

Figure S9. The single-site Langmuir-Freundlich fit for nitrogen in CPO-27-Co at 288 K.

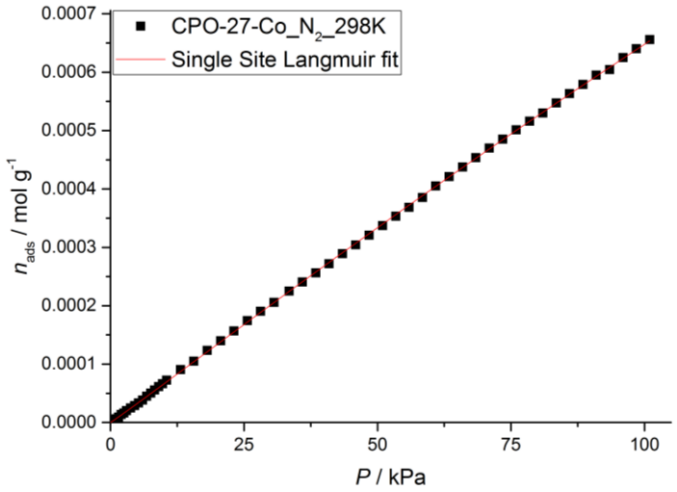

Figure S10. The single-site Langmuir-Freundlich fit for nitrogen in CPO-27-Co at 298 K.

Table S2. The resulting fit parameters for nitrogen uptake in CPO-27-Co.

Param. \ Temp.	273 K	278 K	283 K	288 K	298 K
$n_{sat,1}$	0.0064	0.0064	0.0064	0.0064	0.0064
b_1	0.00191	0.00181	0.00158	0.00126	$9.6712*10^{-4}$
v_1	1.06847	1.03952	1.03029	1.0431	1.03299

Langmuir-Freundlich fits of CPO-27-Co with oxygen:

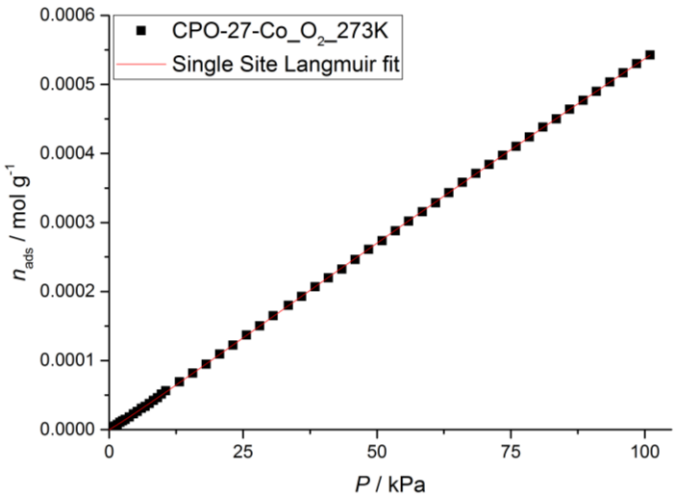

Figure S11. The single-site Langmuir-Freundlich fit for oxygen in CPO-27-Co at 273 K.

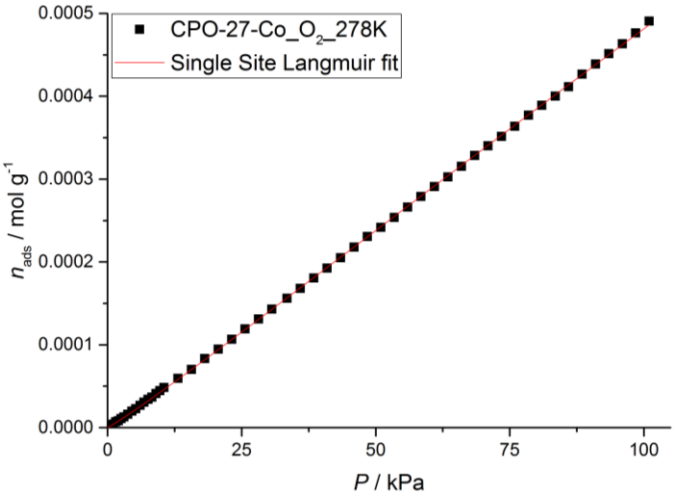

Figure S12. The single-site Langmuir-Freundlich fit for oxygen in CPO-27-Co at 278 K.

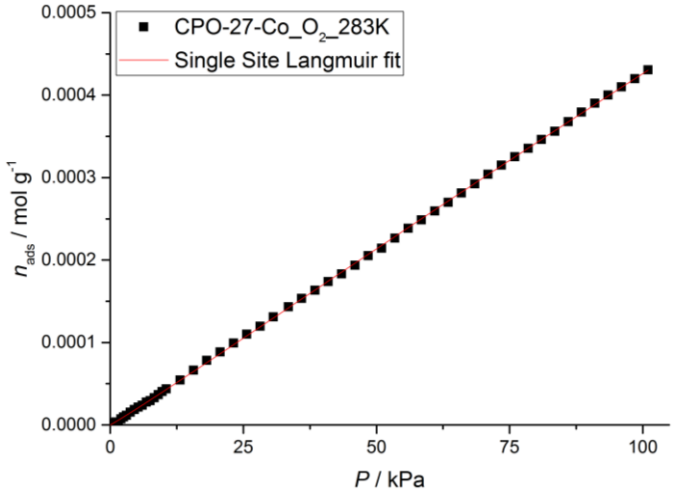

Figure S13. The single-site Langmuir-Freundlich fit for oxygen in CPO-27-Co at 283 K.

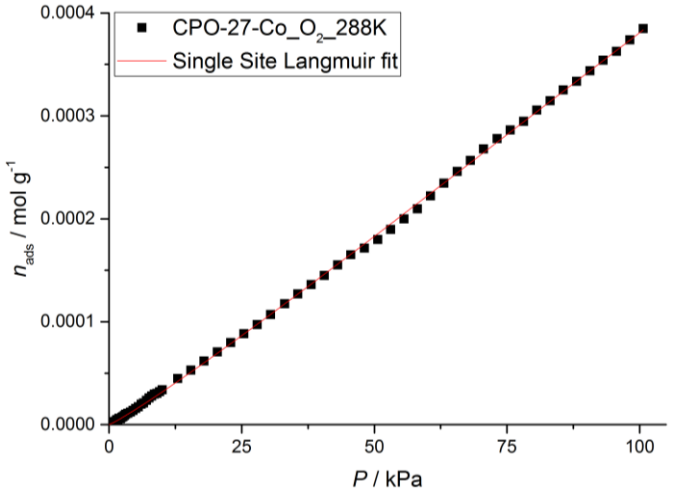

Figure S14. The single-site Langmuir-Freundlich fit for oxygen in CPO-27-Co at 288 K.

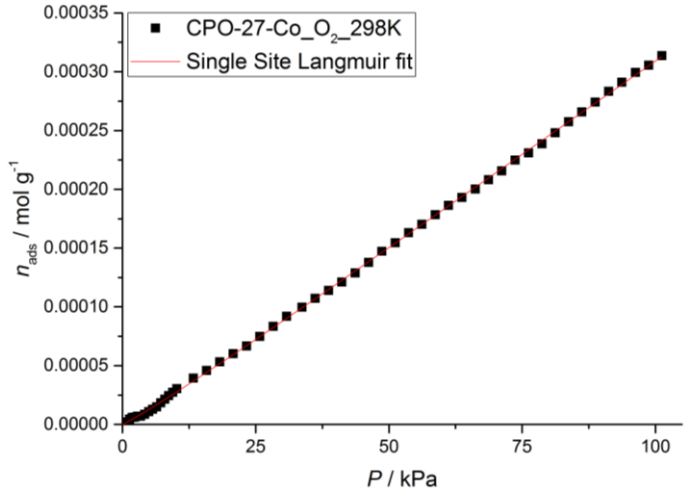

Figure S15. The single-site Langmuir-Freundlich fit for oxygen in CPO-27-Co at 298 K.

Table S3. The resulting fit parameters for oxygen uptake in CPO-27-Co.

Param. \ Temp.	273 K	278 K	283 K	288 K	298 K
$n_{sat,1}$	0.0064	0.0064	0.0064	0.0064	0.0064
b_1	$7.08379*10^{-4}$	$5.77092*10^{-4}$	$5.75684*10^{-4}$	$3.9207*10^{-4}$	$3.58187*10^{-4}$
v_1	1.05587	1.07443	1.04646	1.10388	1.07562

Langmuir-Freundlich fits of CPO-27-Ni with nitrogen:

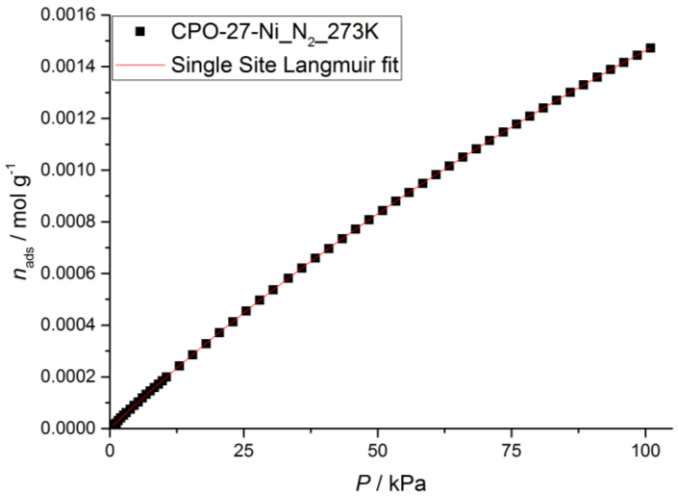

Figure S16. The single-site Langmuir-Freundlich fit for nitrogen in CPO-27-Ni at 273 K.

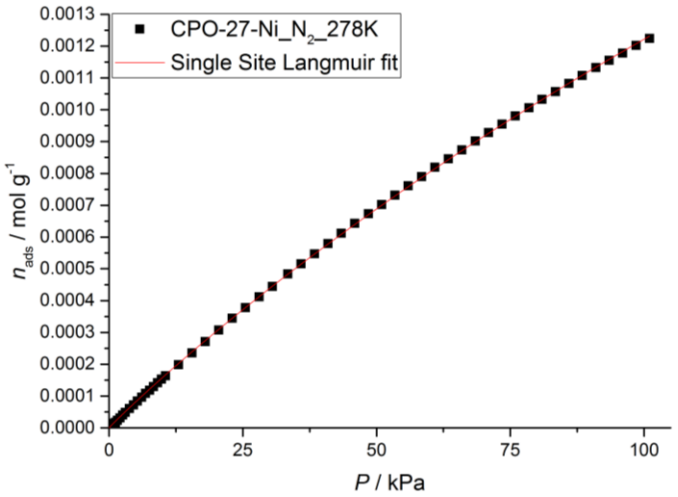

Figure S17. The single-site Langmuir-Freundlich fit for nitrogen in CPO-27-Ni at 278 K.

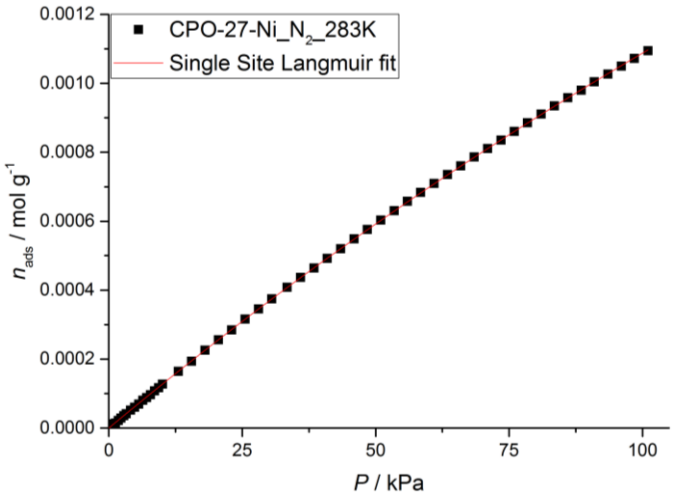

Figure S18. The single-site Langmuir-Freundlich fit for nitrogen in CPO-27-Ni at 283 K.

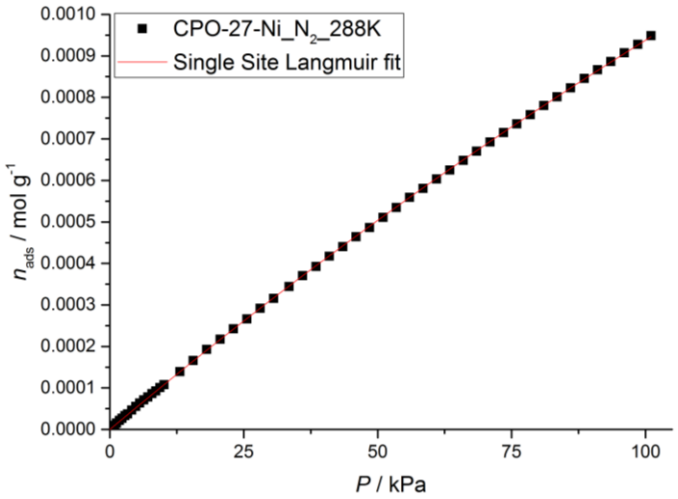

Figure S19. The single-site Langmuir-Freundlich fit for nitrogen in CPO-27-Ni at 288 K.

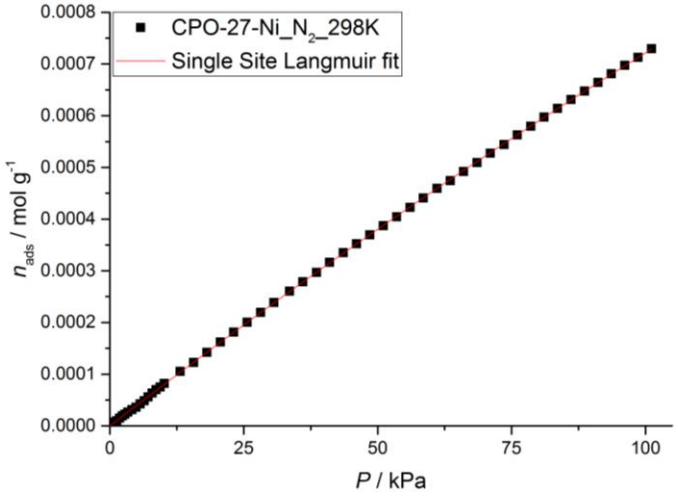

Figure S20. The single-site Langmuir-Freundlich fit for nitrogen in CPO-27-Ni at 298 K.

Table S4. The resulting fit parameters for nitrogen uptake in CPO-27-Ni.

Param. \ Temp.	273 K	278 K	283 K	288 K	298 K
$n_{sat,1}$	0.0064	0.0064	0.0064	0.0064	0.0064
b_1	0.00313	0.00272	0.00199	0.00167	0.00123
v_1	0.98821	0.96885	1.00571	1.00617	1.0075

Langmuir-Freundlich fits of CPO-27-Ni with oxygen:

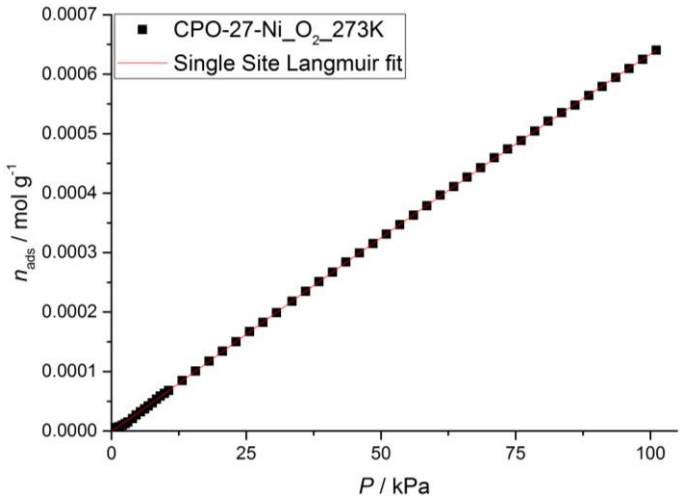

Figure S21. The single-site Langmuir-Freundlich fit for oxygen in CPO-27-Ni at 273 K.

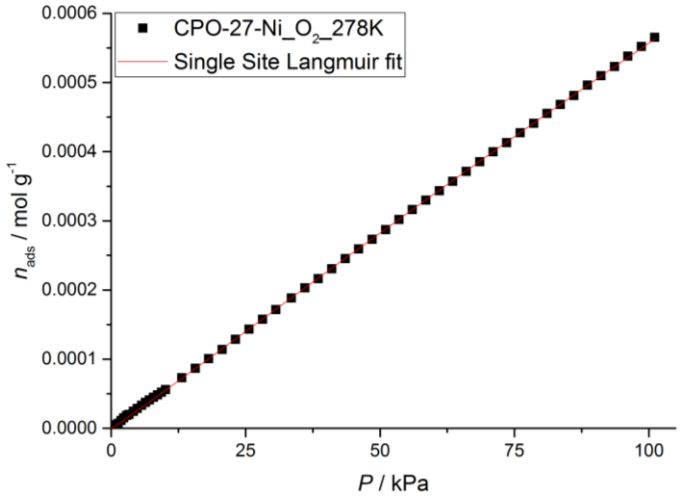

Figure S22. The single-site Langmuir-Freundlich fit for oxygen in CPO-27-Ni at 278 K.

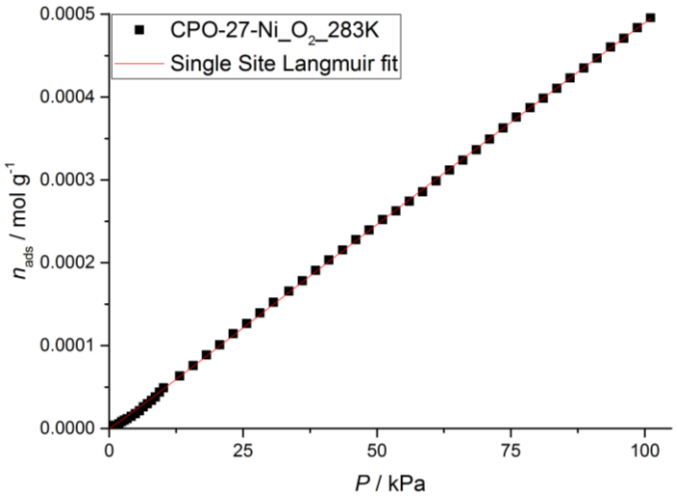

Figure S23. The single-site Langmuir-Freundlich fit for oxygen in CPO-27-Ni at 283 K.

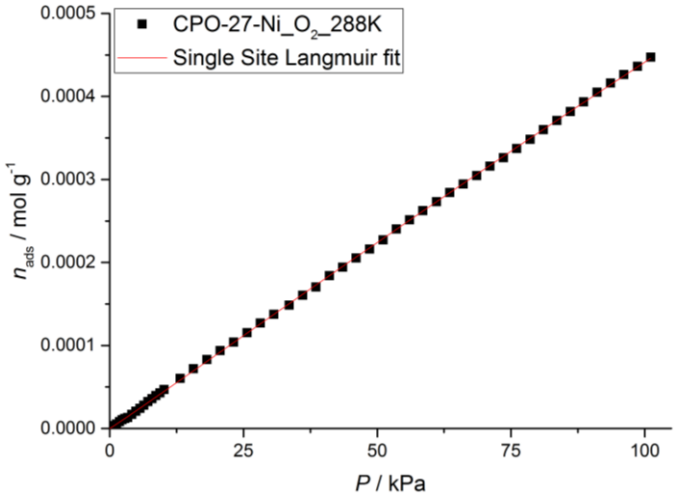

Figure S24. The single-site Langmuir-Freundlich fit for oxygen in CPO-27-Ni at 288 K.

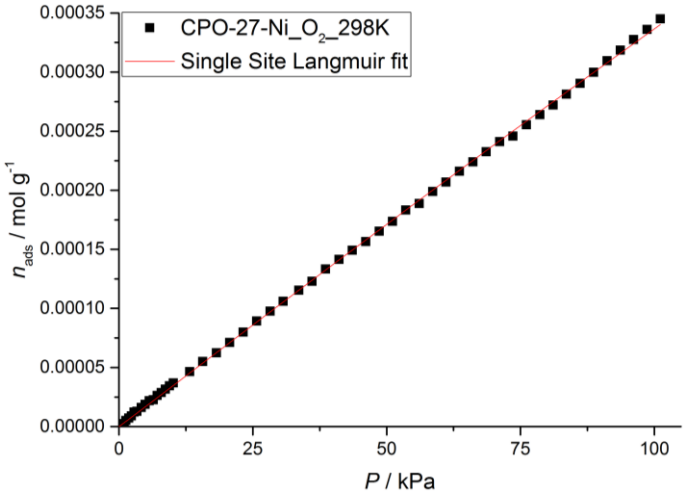

Figure S25. The single-site Langmuir-Freundlich fit for oxygen in CPO-27-Ni at 298 K.

Table S5. The resulting fit parameters for oxygen uptake in CPO-27-Ni.

Param. \ Temp.	273 K	278 K	283 K	288 K	298 K
$n_{sat,1}$	0.0064	0.0064	0.0064	0.0064	0.0064
b_1	$9.20457*10^{-4}$	$7.73025*10^{-4}$	$6.58876*10^{-4}$	$6.46544*10^{-4}$	$5.19125*10^{-4}$
v_1	1.03844	1.04549	1.04975	1.02943	1.01448

Langmuir-Freundlich fits of CPO-27-Mn with nitrogen:

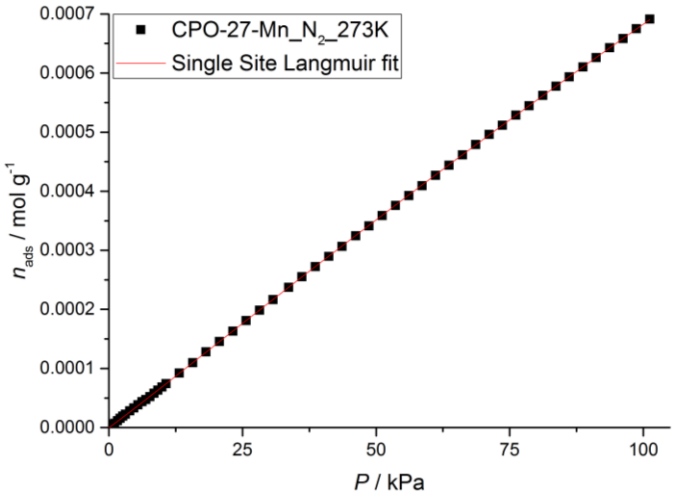

Figure S26. The single-site Langmuir-Freundlich fit for nitrogen in CPO-27-Mn at 273 K.

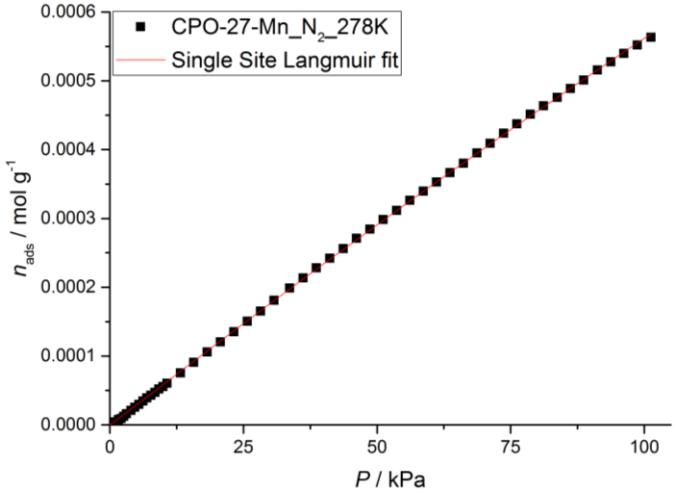

Figure S27. The single-site Langmuir-Freundlich fit for nitrogen in CPO-27-Mn at 278 K.

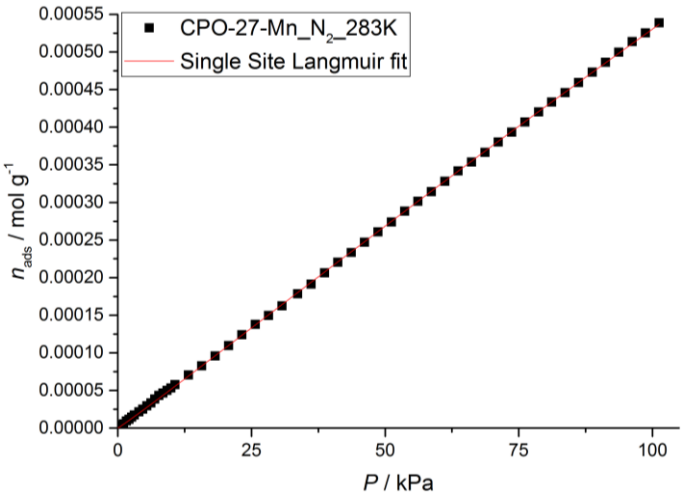

Figure S28. The single-site Langmuir-Freundlich fit for nitrogen in CPO-27-Mn at 283 K.

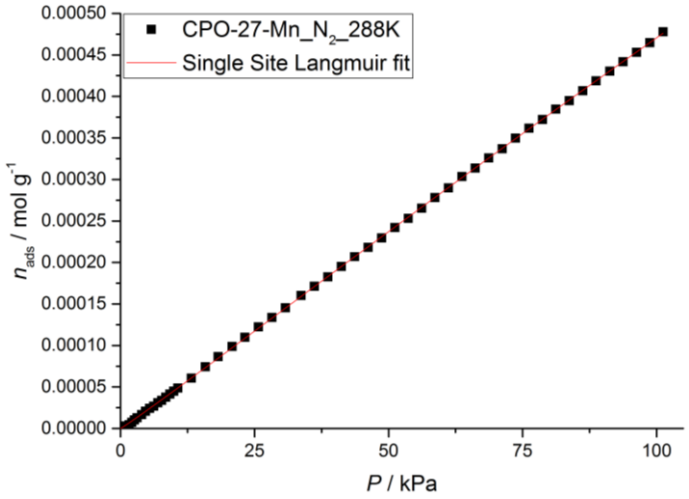

Figure S29. The single-site Langmuir-Freundlich fit for nitrogen in CPO-27-Mn at 288 K.

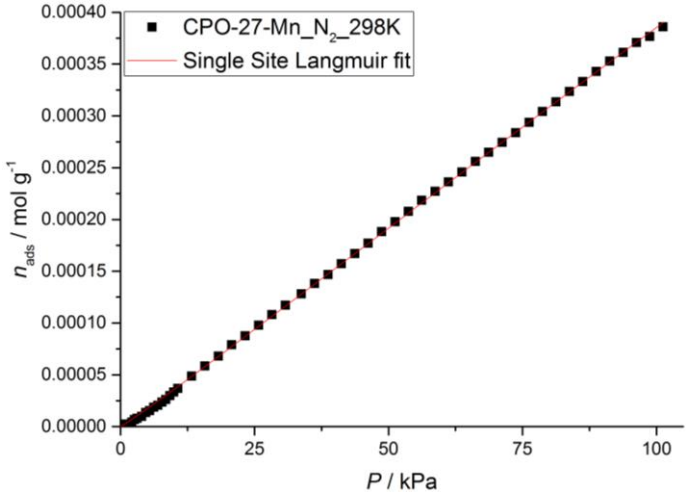

Figure S30. The single-site Langmuir-Freundlich fit for nitrogen in CPO-27-Mn at 298 K.

Table S6. The resulting fit parameters for nitrogen uptake in CPO-27-Mn.

Param. \ Temp.	273 K	278 K	283 K	288 K	298 K
$n_{sat,1}$	0.0064	0.0064	0.0064	0.0064	0.0064
b_1	$9.99626*10^{-4}$	$8.95078*10^{-4}$	$7.35813*10^{-4}$	$6.4749*10^{-4}$	$5.00476*10^{-4}$
v_1	1.03854	1.01563	1.04453	1.04414	1.05361

Langmuir-Freundlich fits of CPO-27-Mn with oxygen:

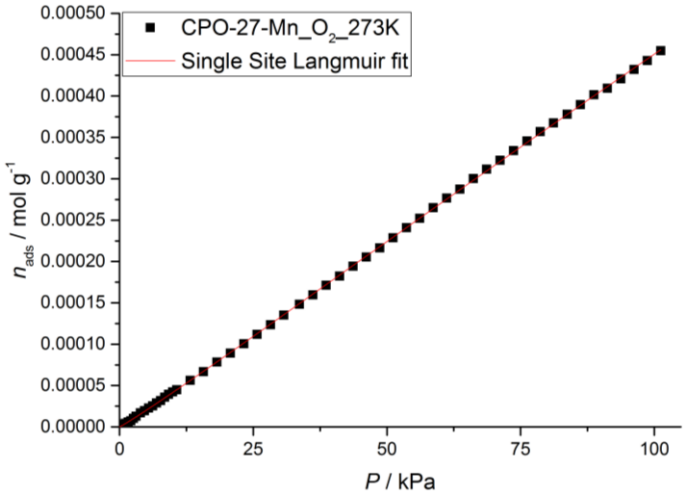

Figure S31. The single-site Langmuir-Freundlich fit for oxygen in CPO-27-Mn at 273 K.

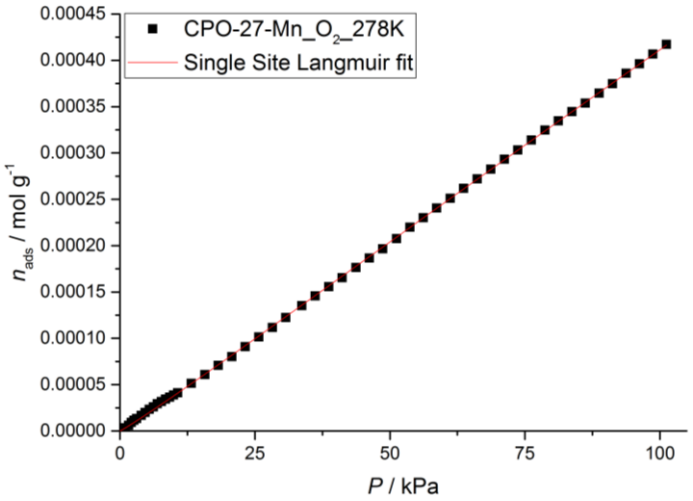

Figure S32. The single-site Langmuir-Freundlich fit for oxygen in CPO-27-Mn at 278 K.

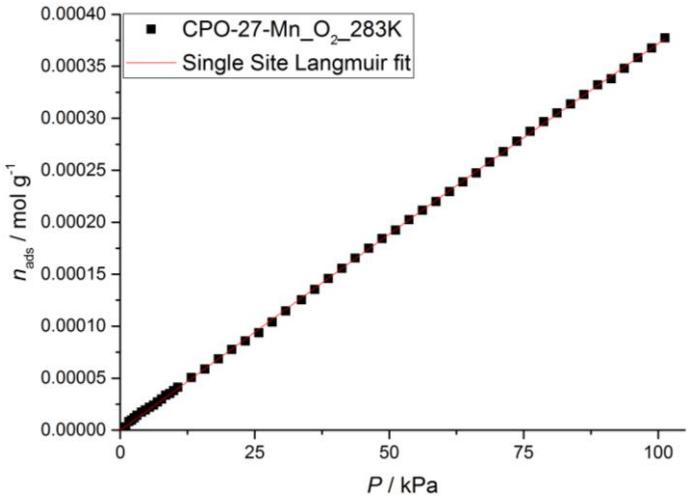

Figure S33. The single-site Langmuir-Freundlich fit for oxygen in CPO-27-Mn at 283 K.

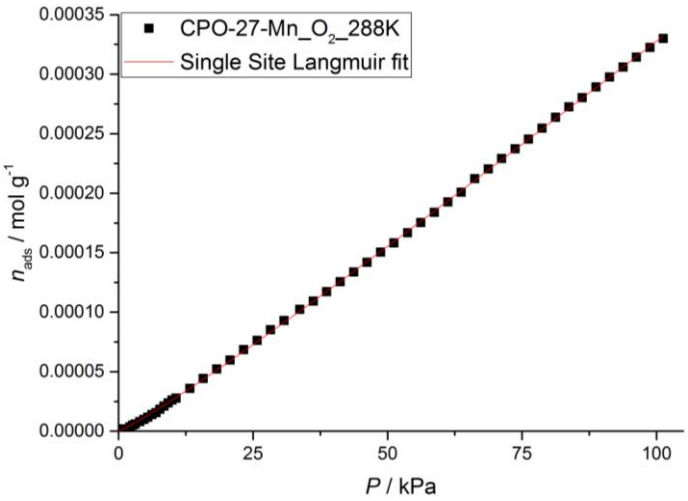

Figure S341. The single-site Langmuir-Freundlich fit for oxygen in CPO-27-Mn at 288 K.

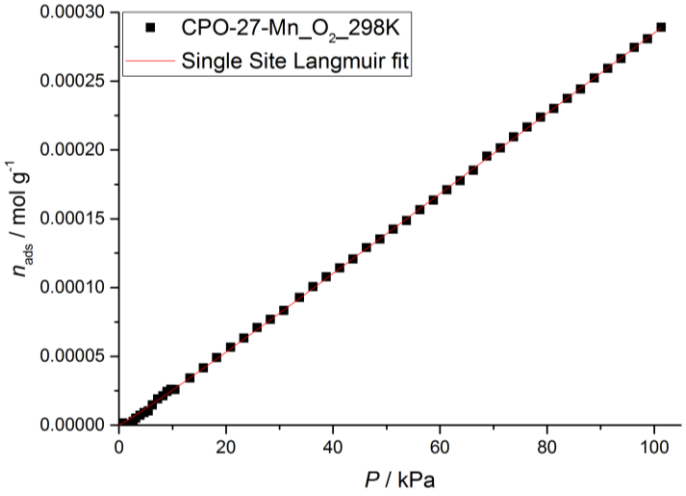

Figure S35. The single-site Langmuir-Freundlich fit for oxygen in CPO-27-Mn at 298 K.

Table S7. The resulting fit parameters for oxygen uptake in CPO-27-Mn.

Param. \ Temp.	273 K	278 K	283 K	288 K	298 K
$n_{sat,1}$	0.0064	0.0064	0.0064	0.0064	0.0064
b_1	$5.71925*10^{-4}$	$5.20763*10^{-4}$	$5.54949*10^{-4}$	$3.16128*10^{-4}$	$3.41428*10^{-4}$
v_1	1.06097	1.06007	1.02301	1.11605	1.06748

Langmuir-Freundlich fits of CPO-27-Cu with nitrogen:

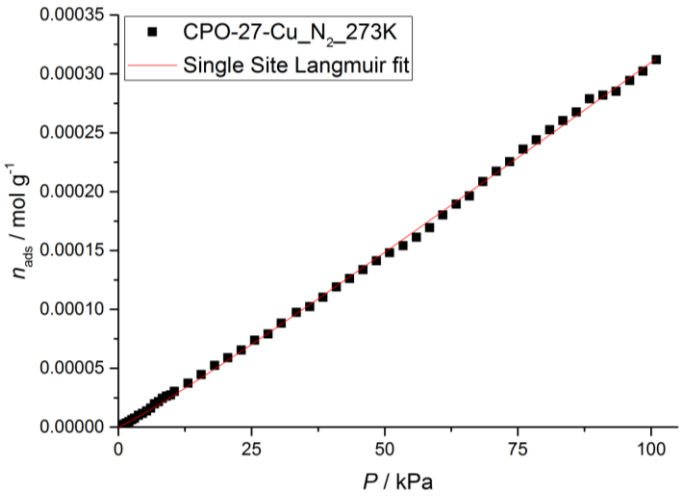

Figure S36. The single-site Langmuir-Freundlich fit for nitrogen in CPO-27-Cu at 273 K.

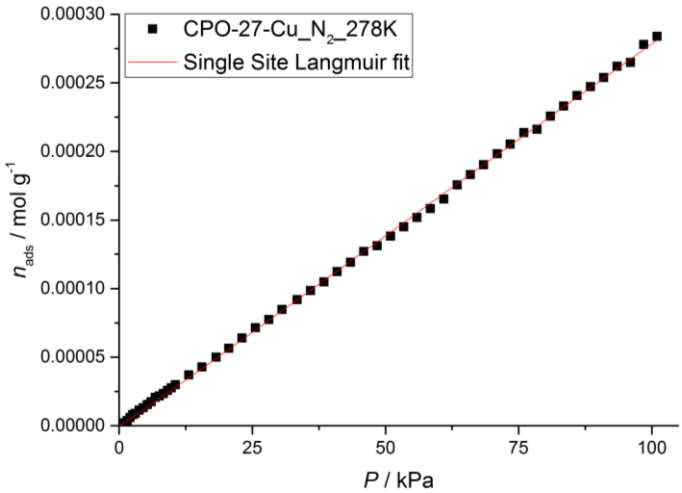

Figure S37. The single-site Langmuir-Freundlich fit for nitrogen in CPO-27-Cu at 278 K.

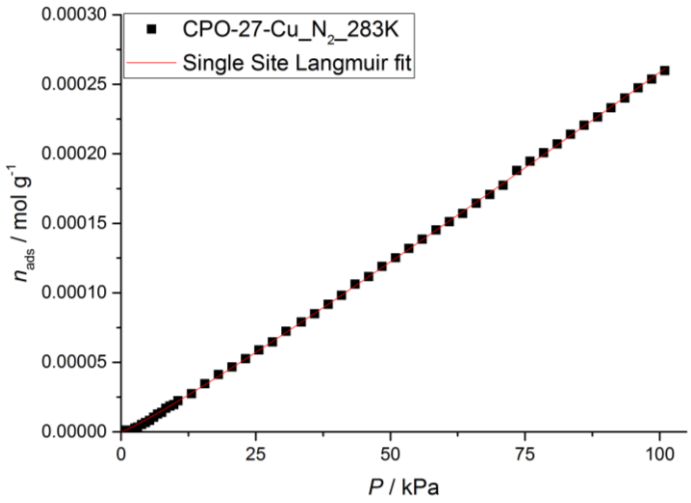

Figure S38. The single-site Langmuir-Freundlich fit for nitrogen in CPO-27-Cu at 283 K.

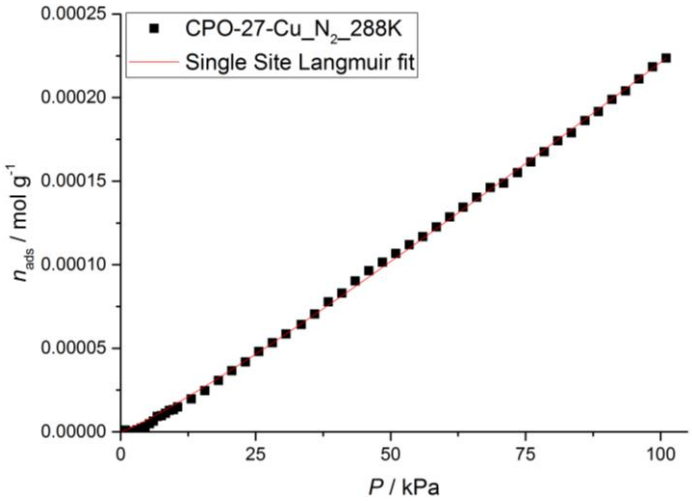

Figure S39. The single-site Langmuir-Freundlich fit for nitrogen in CPO-27-Cu at 288 K.

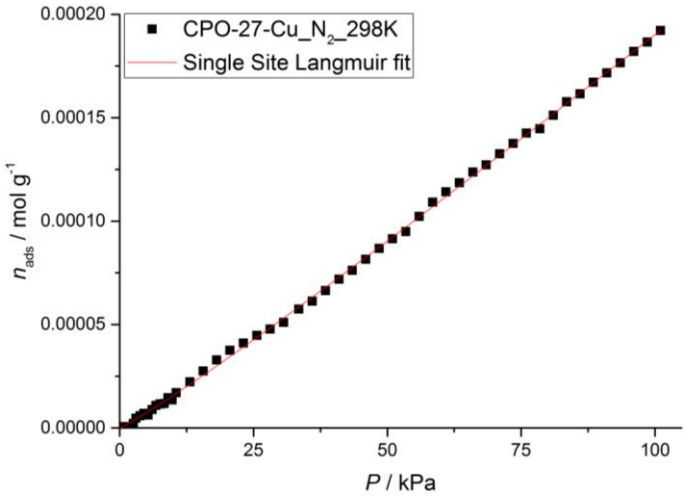

Figure S40. The single-site Langmuir-Freundlich fit for nitrogen in CPO-27-Cu at 298K.

Table S8. The resulting fit parameters for nitrogen uptake in CPO-27-Cu.

Param. \ Temp.	273 K	278 K	283 K	288 K	298 K
$n_{sat,1}$	0.0064	0.0064	0.0064	0.0064	0.0064
b_1	$3.23975*10^{-4}$	$3.77302*10^{-4}$	$2.51927*10^{-4}$	$1.83584*10^{-4}$	$1.96623*10^{-4}$
v_1	1.09789	1.04058	1.11148	1.14485	1.09614

Langmuir-Freundlich fits of CPO-27-Cu with oxygen:

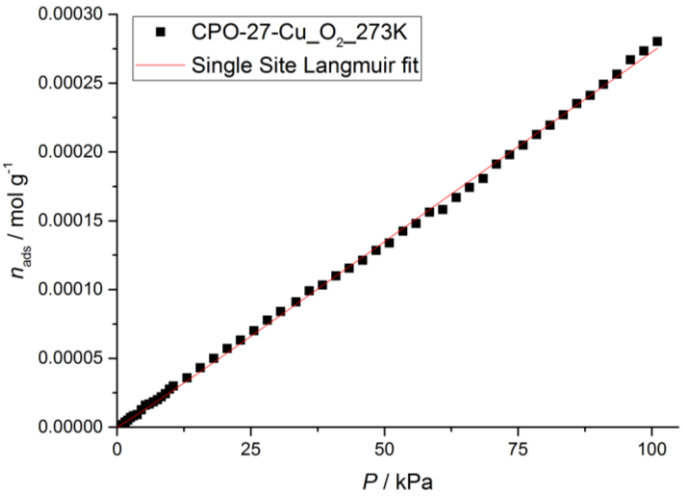

Figure S41. The single-site Langmuir-Freundlich fit for oxygen in CPO-27-Cu at 273 K.

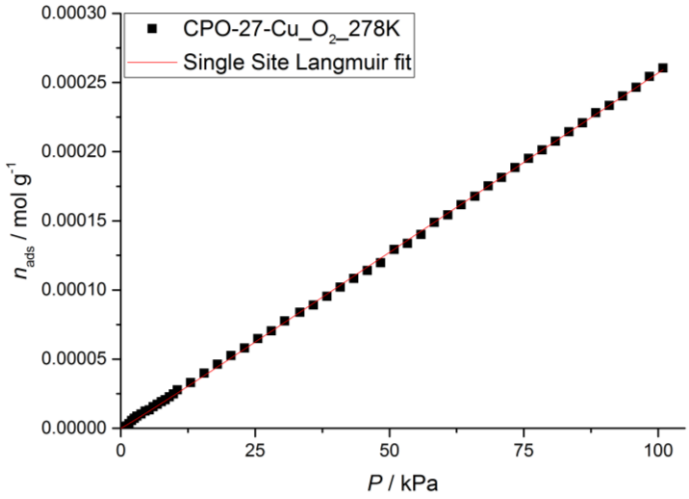

Figure S42. The single-site Langmuir-Freundlich fit for oxygen in CPO-27-Cu at 278 K.

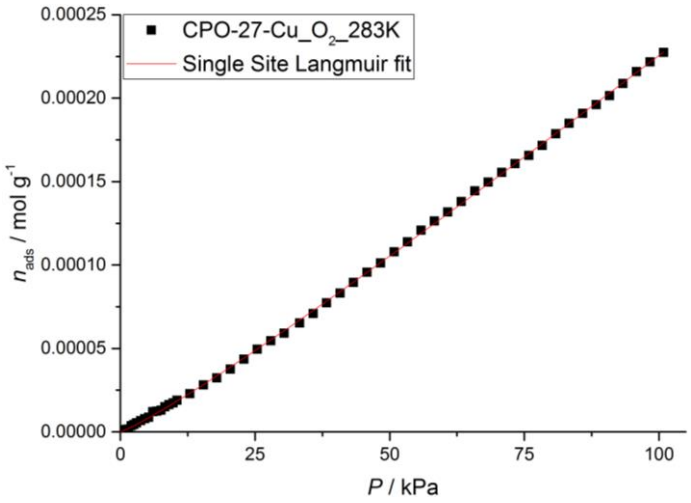

Figure S43. The single-site Langmuir-Freundlich fit for oxygen in CPO-27-Cu at 283 K.

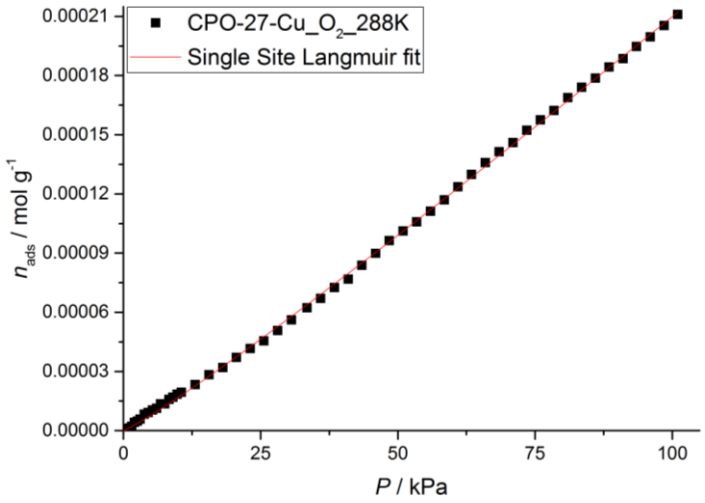

Figure S44. The single-site Langmuir-Freundlich fit for oxygen in CPO-27-Cu at 288 K.

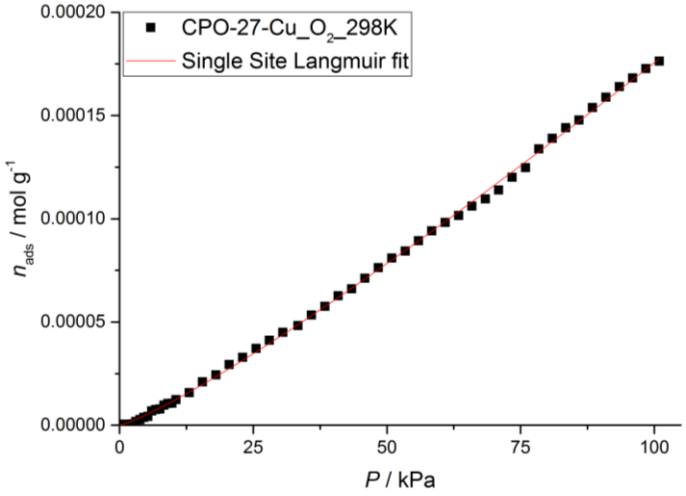

Figure S45. The single-site Langmuir-Freundlich fit for oxygen in CPO-27-Cu at 298 K.

Table S9. The resulting fit parameters for oxygen uptake in CPO-27-Cu.

Param. \ Temp.	273 K	278 K	283 K	288 K	298 K
$n_{sat,1}$	0.0064	0.0064	0.0064	0.0064	0.0064
b_1	$3.58396*10^{-4}$	$3.42074*10^{-4}$	$2.04671*10^{-4}$	$2.05911*10^{-4}$	$1.19181*10^{-4}$
v_1	1.04682	1.04358	1.12575	1.10824	1.18701

Langmuir-Freundlich fits of CPO-27-Zn with nitrogen:

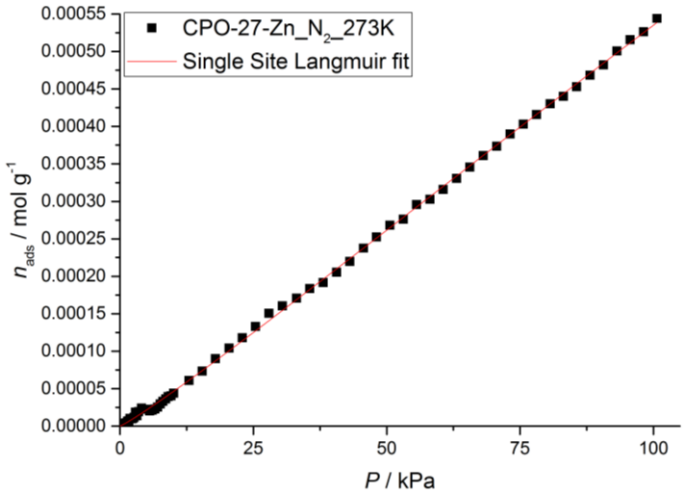

Figure S46. The single-site Langmuir-Freundlich fit for nitrogen in CPO-27-Zn at 273 K.

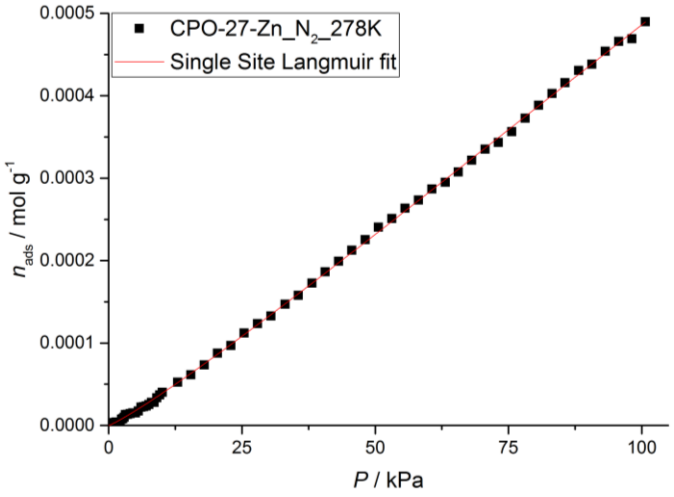

Figure S47. The single-site Langmuir-Freundlich fit for nitrogen in CPO-27-Zn at 278 K.

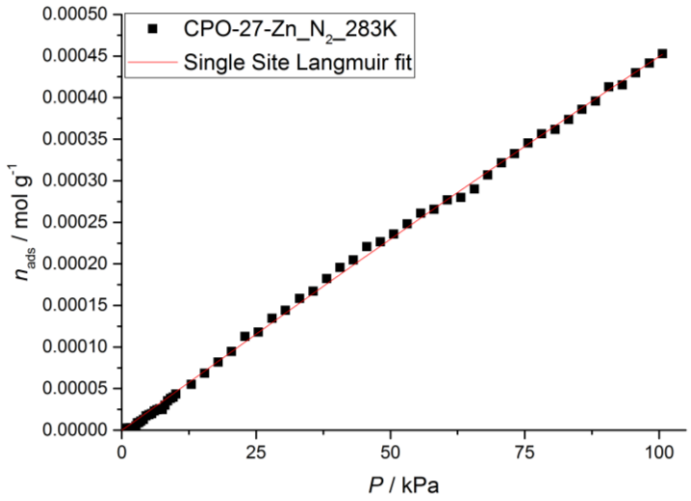

Figure S48. The single-site Langmuir-Freundlich fit for nitrogen in CPO-27-Zn at 283 K.

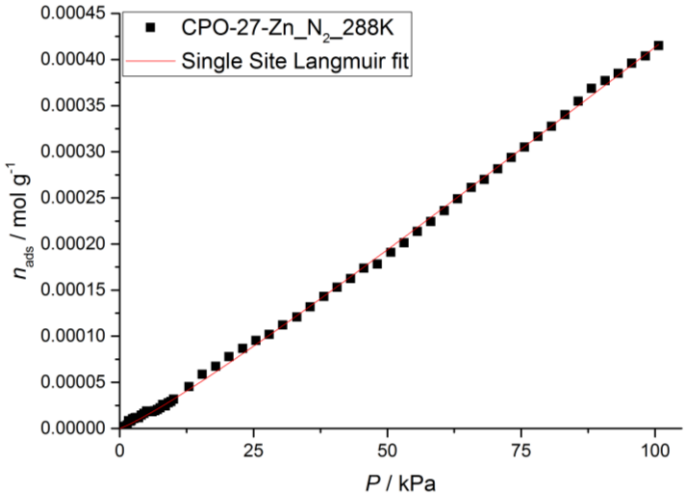

Figure S49. The single-site Langmuir-Freundlich fit for nitrogen in CPO-27-Zn at 288 K.

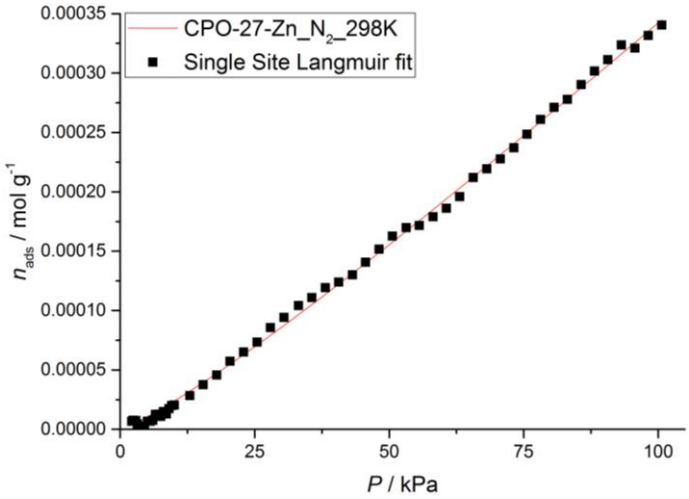

Figure S50. The single-site Langmuir-Freundlich fit for nitrogen in CPO-27-Zn at 298 K.

Table S10. The resulting fit parameters for nitrogen uptake in CPO-27-Zn.

Param. \ Temp.	273 K	278 K	283 K	288 K	298 K
$n_{sat,1}$	0.0064	0.0064	0.0064	0.0064	0.0064
b_1	$5.80769*10^{-4}$	$4.5461*10^{-4}$	$6.89797*10^{-4}$	$3.5523*10^{-4}$	$2.44555*10^{-4}$
v_1	1.09799	1.12849	1.01959	1.14423	1.1817

Langmuir-Freundlich fits of CPO-27-Zn with oxygen:

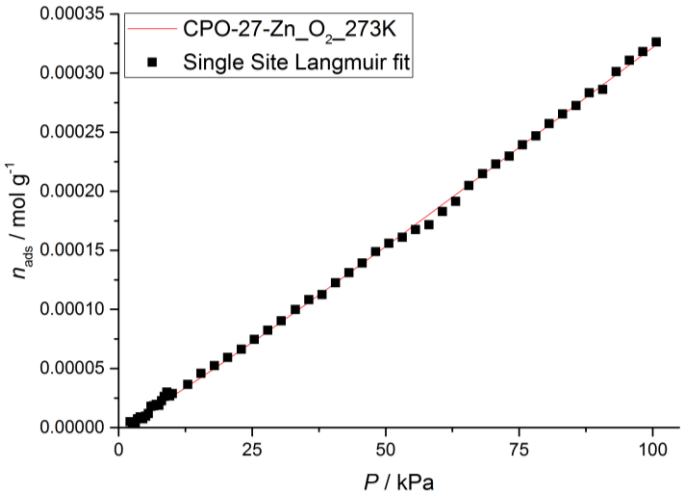

Figure S51. The single-site Langmuir-Freundlich fit for oxygen in CPO-27-Zn at 273 K.

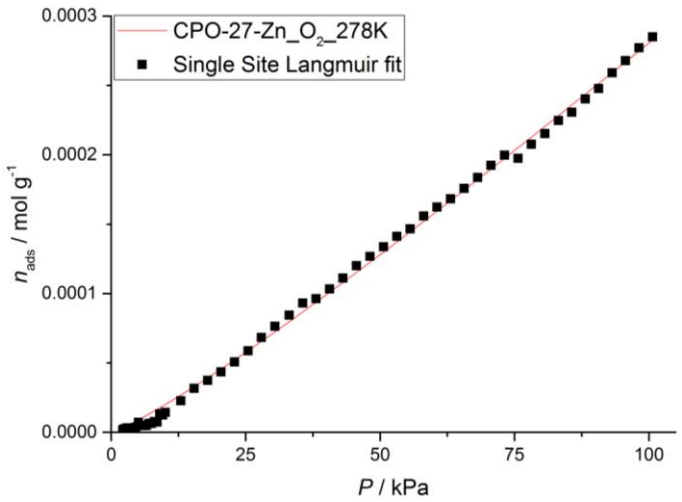

Figure S52. The single-site Langmuir-Freundlich fit for oxygen in CPO-27-Zn at 278 K.

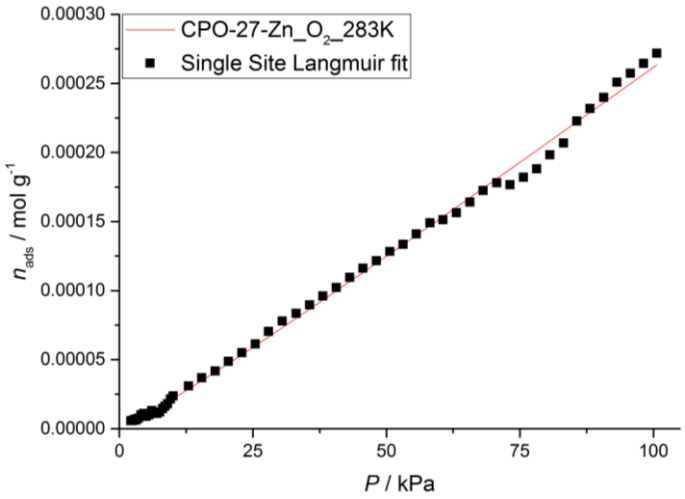

Figure S53. The single-site Langmuir-Freundlich fit for oxygen in CPO-27-Zn at 283 K.

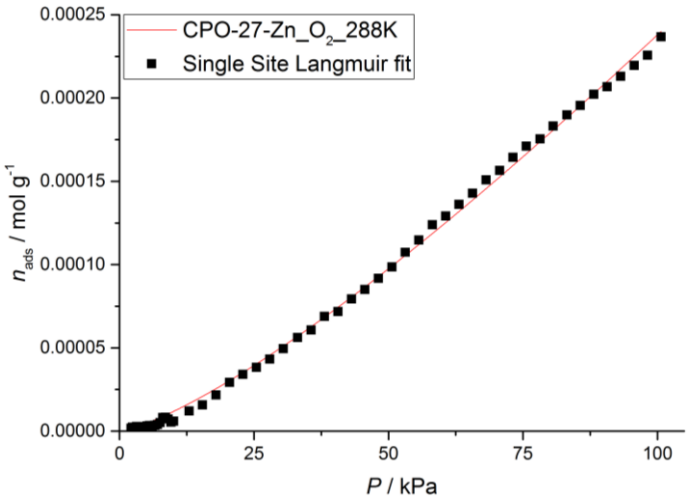

Figure S54. The single-site Langmuir-Freundlich fit for oxygen in CPO-27-Zn at 288 K.

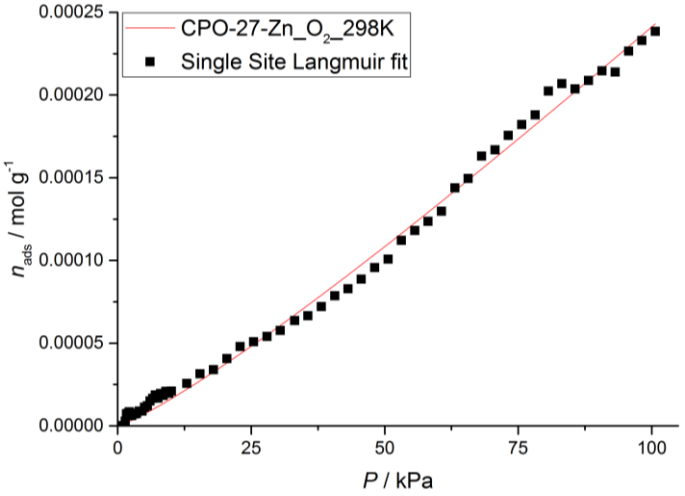

Figure S55. The single-site Langmuir-Freundlich fit for oxygen in CPO-27-Zn at 298 K.

Table S11. The resulting fit parameters for oxygen uptake in CPO-27-Zn.

Param. \ Temp.	273 K	278 K	283 K	288 K	298 K
$n_{sat,1}$	0.0064	0.0064	0.0064	0.0064	0.0064
b_1	$3.21424*10^{-4}$	$2.11999*10^{-4}$	$2.7063*10^{-4}$	$8.8689*10^{-5}$	$1.67266*10^{-4}$
v_1	1.1082	1.1674	1.09858	1.31936	1.18465

Isosteric Heat of Adsorption

The coverage dependent isosteric heat of adsorption, Q_{st}, was calculated for each of the compounds, for both N_2 and O_2, by taking equally spaced points from the isotherm single-site Langmuir-Freundlich fits and using the modified Clausius-Clapeyron equation (Equation 3), whose linear form (Equation 4) was used to fit to the corresponding ln *P* vs. 1/*T* isotherm data at each fractional coverage point θ.

For all the compounds, the calculations started at $5 \cdot 10^{-5}$ mol g^{-1}, whereas the upper limit was decided by the maximum n_{ads} for which data from the four temperatures were still available, and hence varied for the different compounds and gas adsorbed. The resulting isosteric heats of adsorption of nitrogen and oxygen in CPO-27-M is shown in Figure S56 and S57, respectively.

Equation 3. Modified Clausius-Clapeyron equation for Q_{st}.

$$Q_{st} = RT^2 \left(\frac{\delta \, lp(P)}{\delta \, T} \right)_{\theta}$$

Equation 4. Linear (integral) form of the above for the Q_{st} fits.

$$\ln P_g = -\frac{1}{T}\frac{Q_{st}}{R} \quad + \quad const$$

Table S12. Parameters used in equation 3.

Parameter	Definition
Q_{st}	Isosteric heat of adsorption, kJ mol^{-1}
R	Gas constant, 8.314462 J K^{-1} mol^{-1}
T	Absolute temperature, K
θ	Fractional coverage

Q_{st} values averaged over the probed range of coverage for both N_2 and O_2 and the five members of the CPO-27 series are listed in Table 13. We observe that CPO-27-Co, Ni, Mn and Zn all have higher isosteric heats of adsorption for nitrogen than for oxygen. The largest difference is observed for the Ni member of the series, with a difference of 7 kJ mol^{-1}, followed by Co at 5 kJ mol^{-1}, and Mn at 3 kJ mol^{-1}. CPO-27-Cu and Zn appear to have very similar heats of adsorption for N_2, whereas there is a clearer difference for O_2.

Table S13. The isosteric heat of adsorption of nitrogen and oxygen on CPO-27-M.

Q_{st} / Compound	Q_{st}, N_2 / kJ mol^{-1}	Q_{st}, O_2 / kJ mol^{-1}
CPO-27-Co	21.2±0.1	15.6±0.1
CPO-27-Ni	23.7±0.1	17.0±0.1
CPO-27-Mn	16.1±0.2	13.3±0.3
CPO-27-Cu	13.5±0.4	13.5±0.3
CPO-27-Zn	12.5±0.3	8.6±0.8

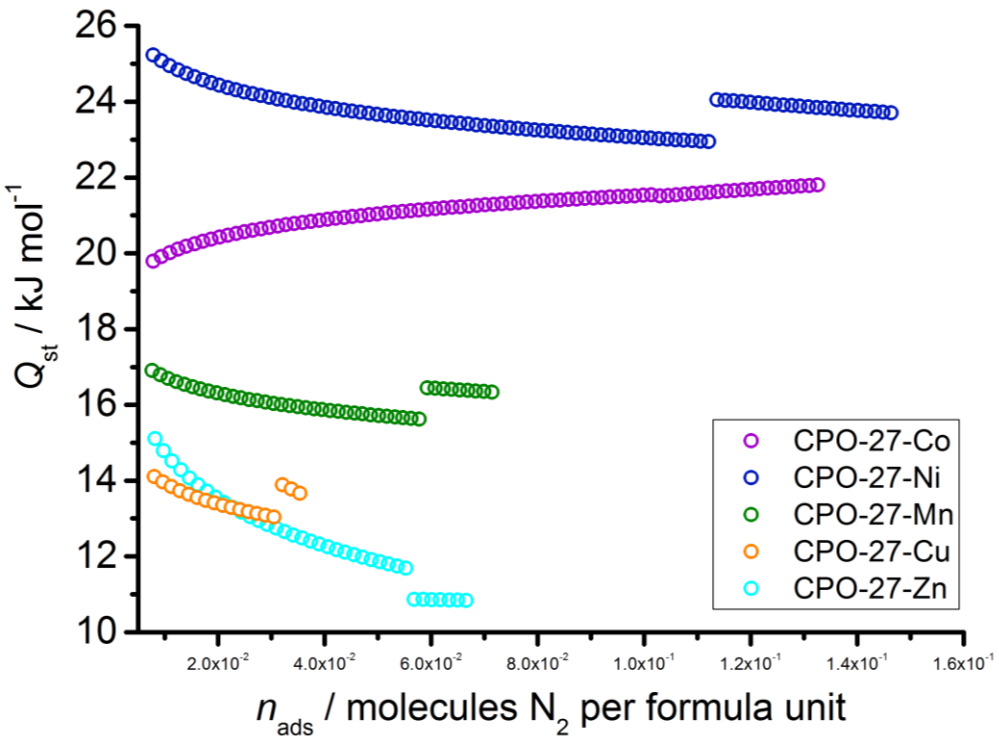

Figure S56. Comparison of nitrogen affinity (quantified as the isosteric heat of adsorption, Q_{st}) for CPO-27–M, where M = Ni (blue), Co (pink), Mn (green), Cu (orange) and Zn (light blue).

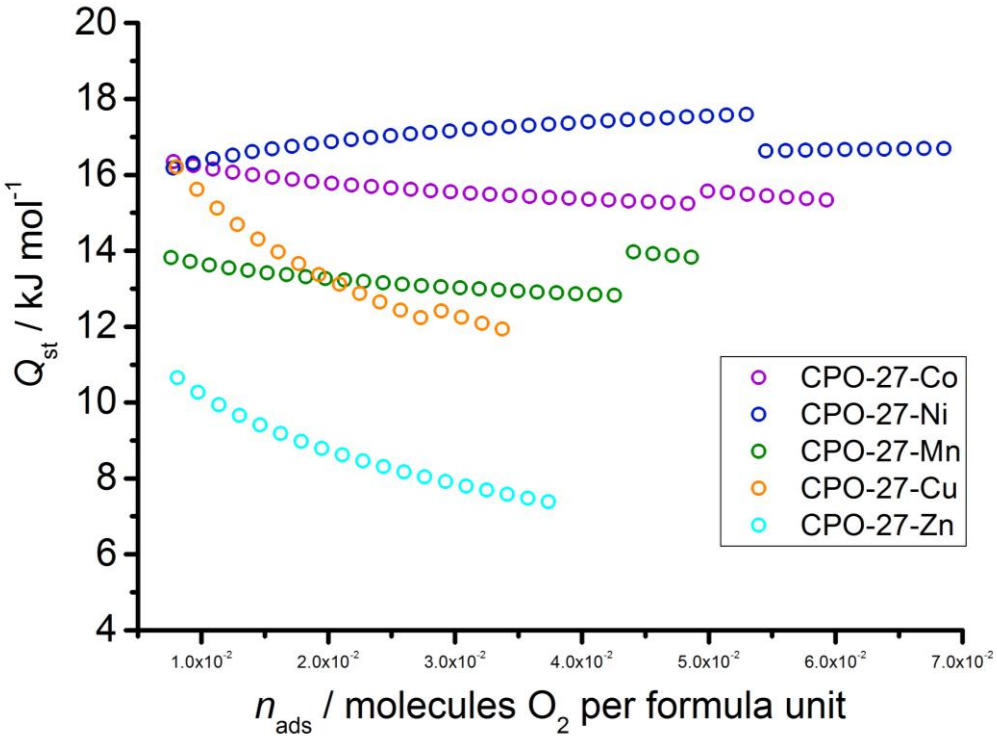

Figure S57. Comparison of oxygen affinity (quantified as the isosteric heat of adsorption, Q_{st}) for CPO-27–M, where M = Ni (blue), Co (pink), Mn (green), Cu (orange) and Zn (light blue).

Rietveld refinement plots

CPO-27-Mn

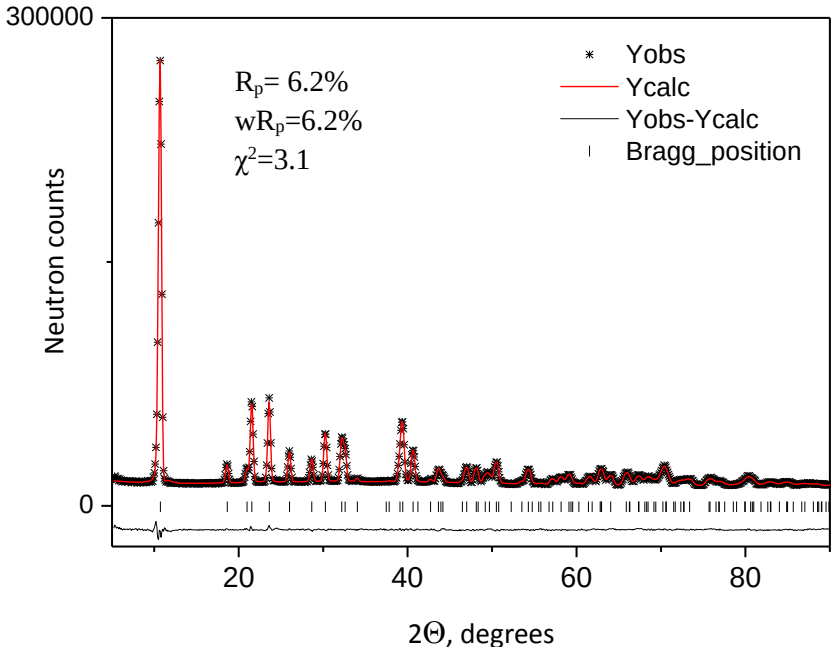

Figure S58. Refinement plot of the CPO-27-Mn material, dosed with 0.33 O_2 per Mn. DMC data, measured at 20 K.

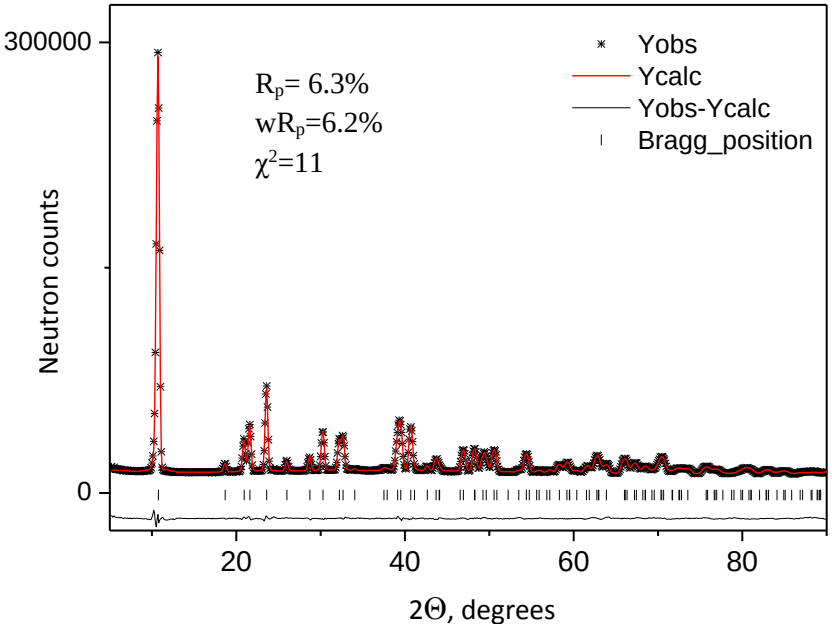

Figure S59. Refinement plot of the CPO-27-Mn material, dosed with 1 O_2 per Mn. DMC data, measured at 20 K.

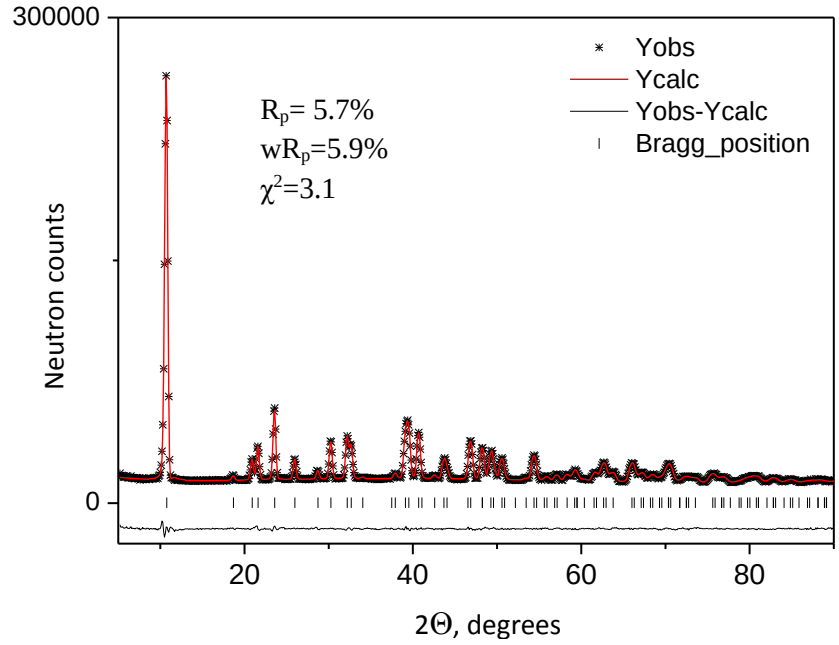

Figure S60. Refinement plot of the CPO-27-Mn material, dosed with 2 O_2 per Mn. DMC data, measured at 20 K.

CPO-27-Co

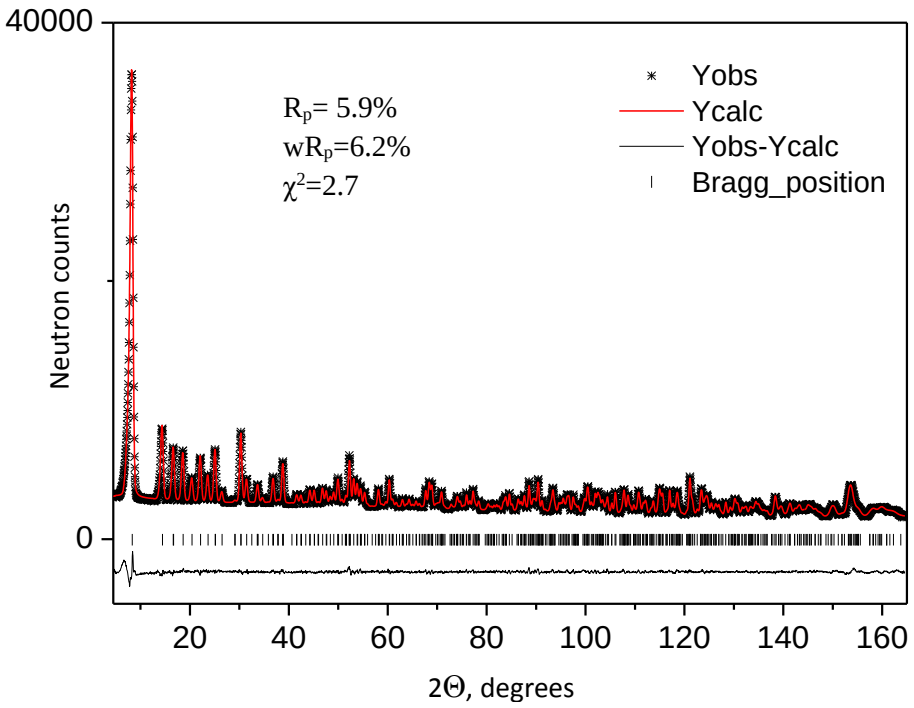

Figure S61. Refinement plot of the fully desolvated CPO-27-Co material. HRPT data, measured at 15 K.

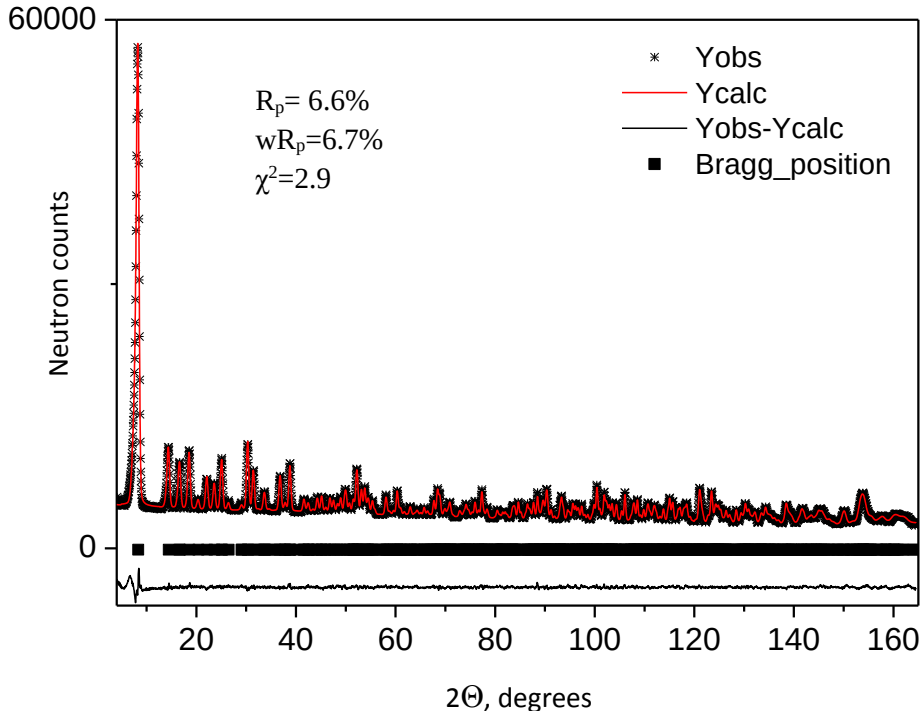

Figure S62. Refinement plot of CPO-27-Co dosed with 0.5O_2 molecule per Co centre . HRPT data, measured at 15 K.

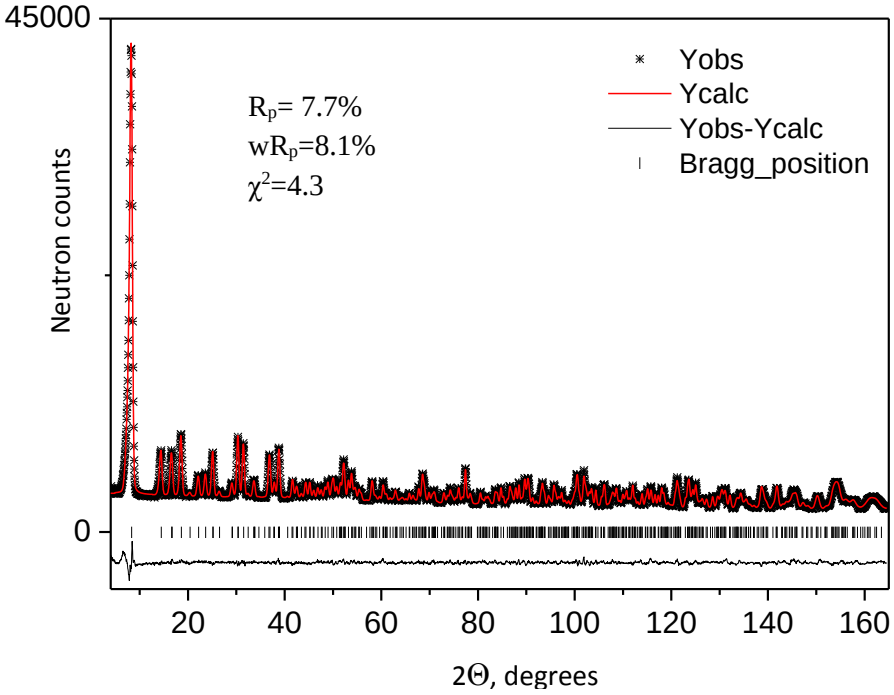

Figure S63. Refinement plot of CPO-27-Co dosed with $1O_2$ molecule per Co. HRPT data, measured at 15 K.

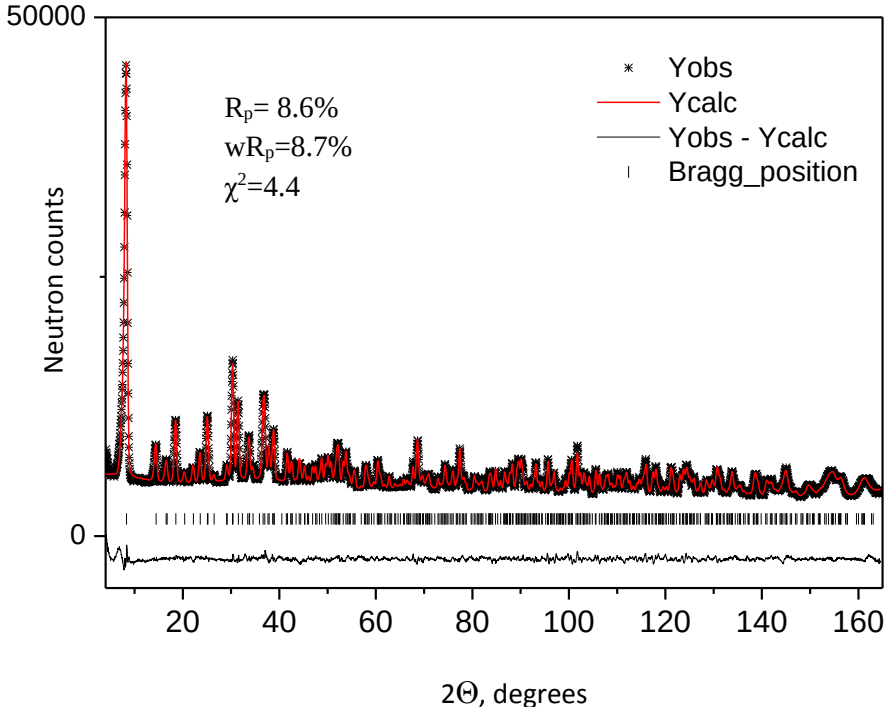

Figure S64. Refinement plot of CPO-27-Co dosed with $2.4O_2$ molecule per Co. HRPT data, measured at 15 K.

CPO-27-Ni

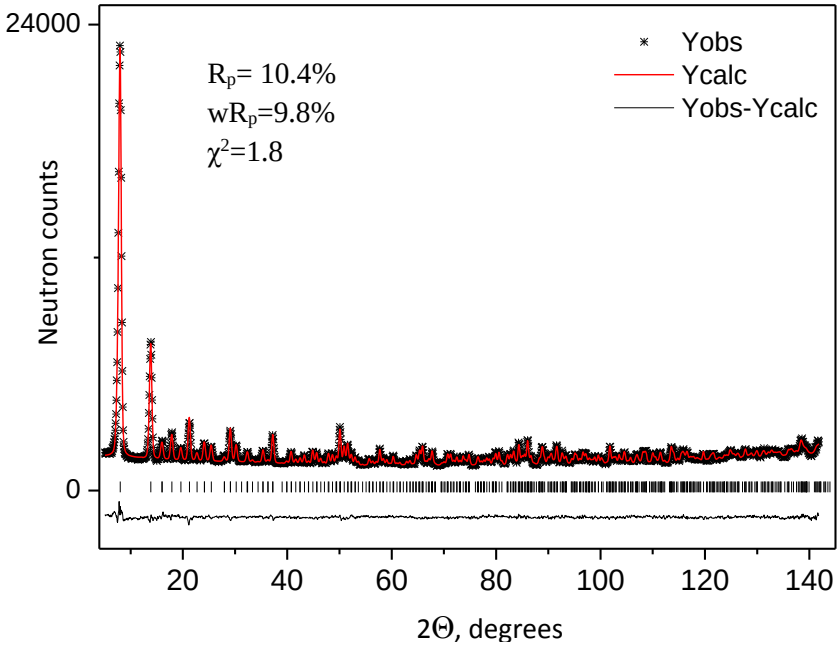

Figure S65. Refinement plot of the fully desolvated CPO-27-Ni material. E9 data, measured at 20 K.

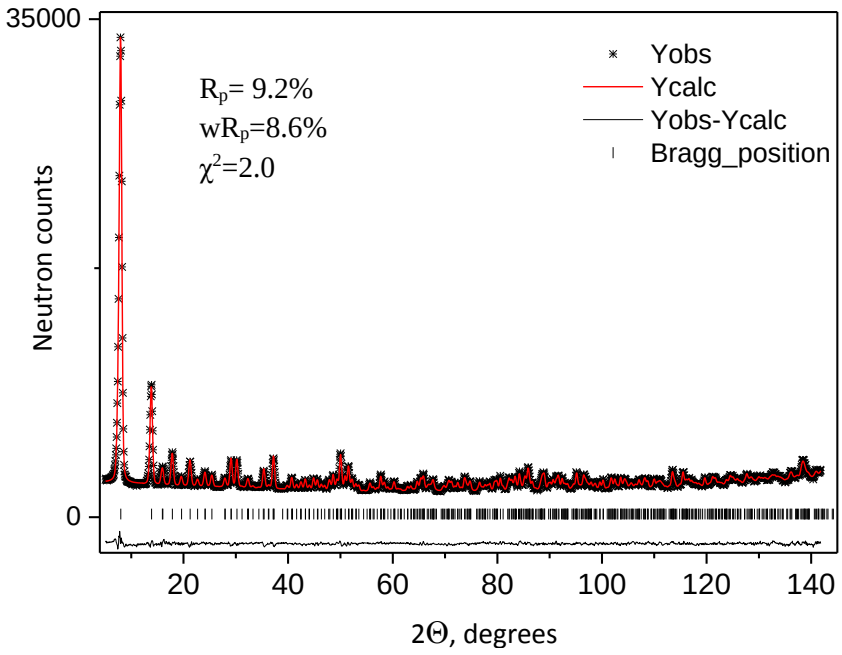

Figure S66. Refinement plot of CPO-27-Ni with $0.5O_2$ per Ni. E9 data, measured at 20 K.

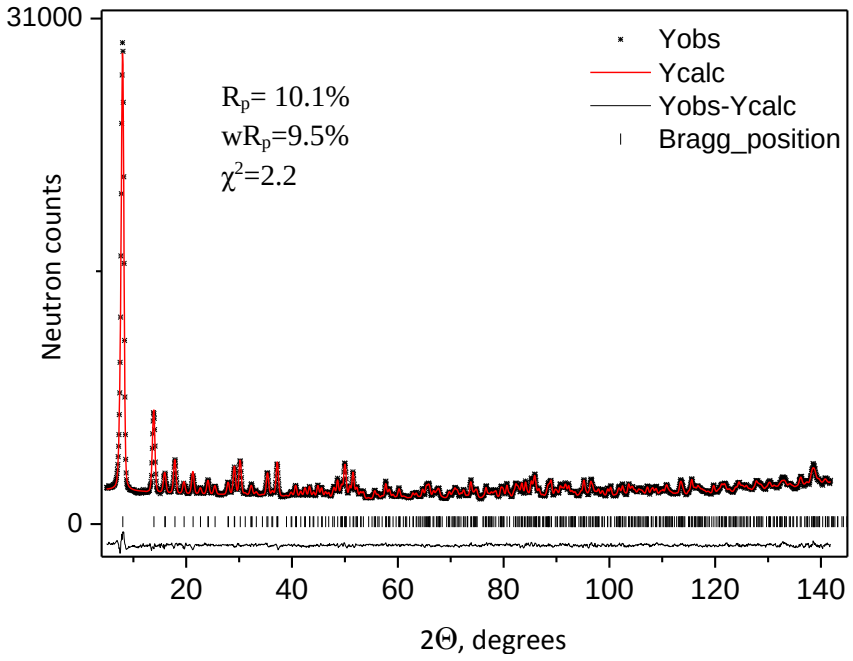

Figure S67. Refinement plot of CPO-27-Ni with $1O_2$ per Ni. E9 data, measured at 20 K.

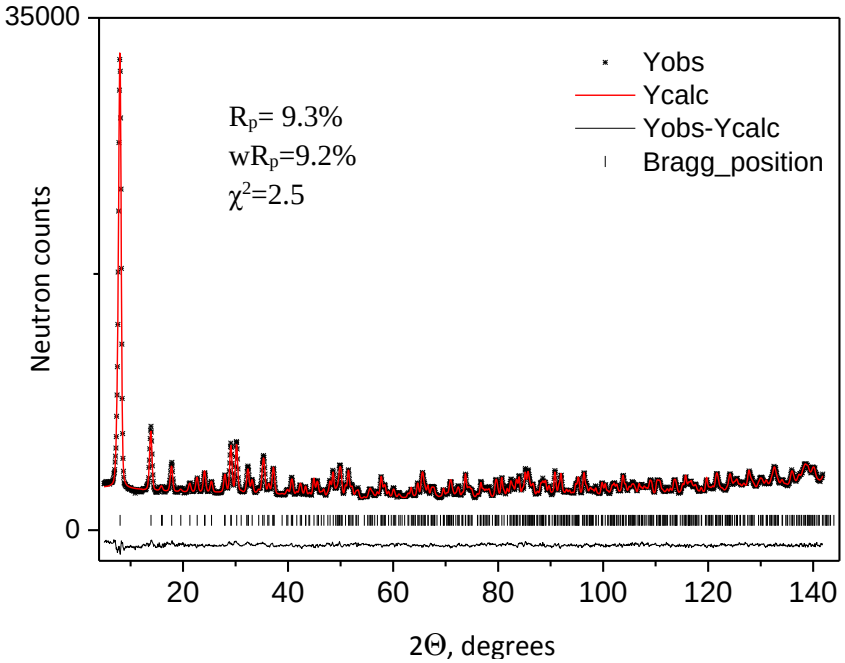

Figure S68: Refinement plot of CPO-27-Ni with $1.8O_2$ per Ni. E9 data, measured at 20 K.

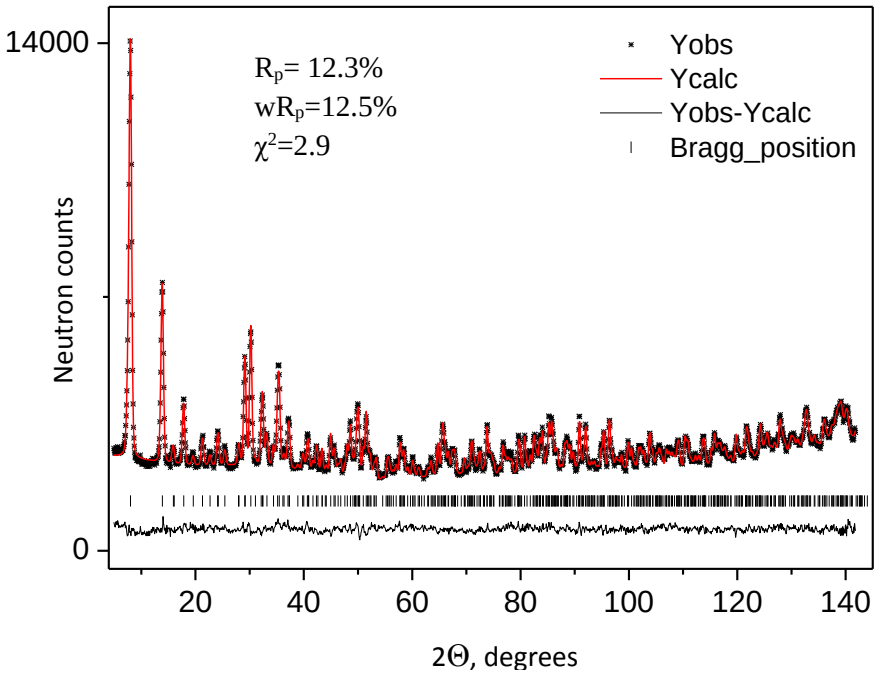

Figure S69. Refinement plot of CPO-27-Ni with 2.6O_2 per Ni. E9 data, measured at 20 K.

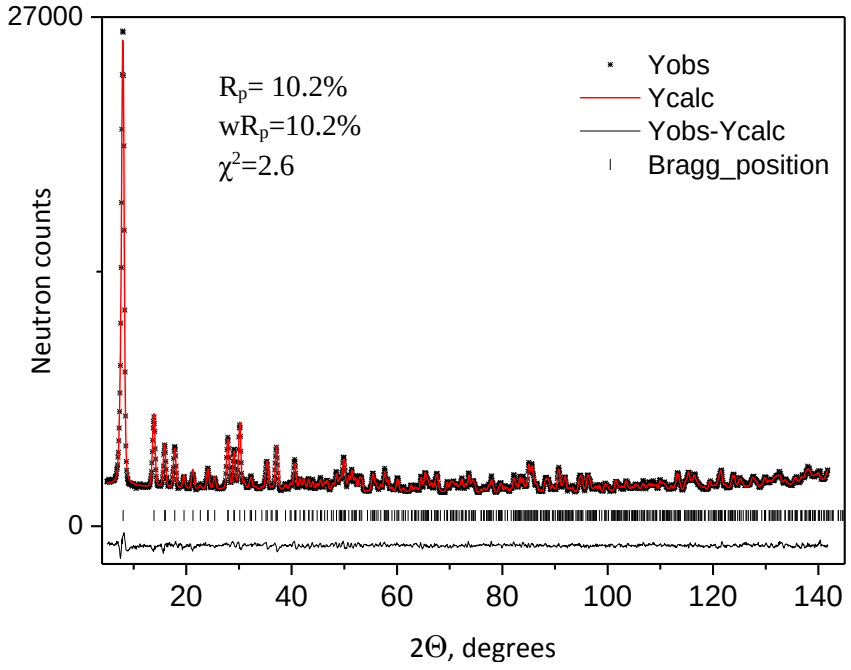

Figure S70. Refinement plot of CPO-27-Ni with 1N_2 per Ni. E9 data, measured at 20 K.

CPO-27-Cu

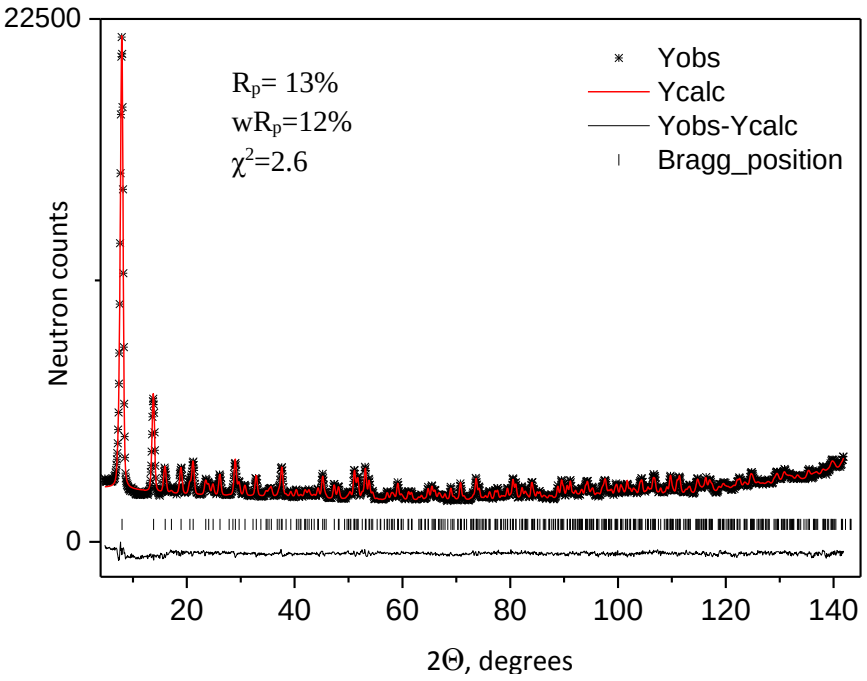

Figure S71. Refinement plot of fully desolvated CPO-27-Cu. E9 data, measured at 15 K.

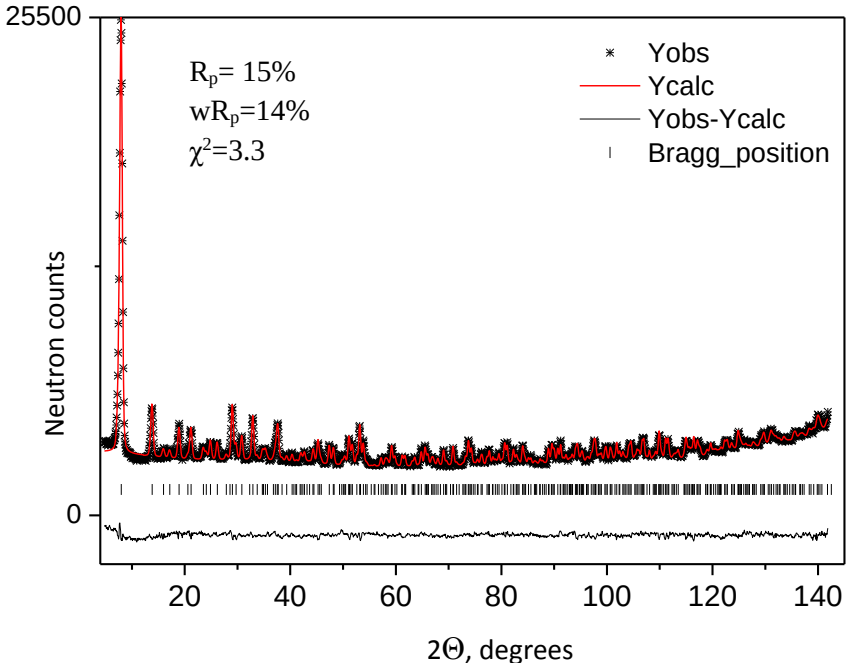

Figure S72. Refinement plot of CPO-27-Cu, loaded with $1O_2$ per Cu. E9 data, measured at 15 K.

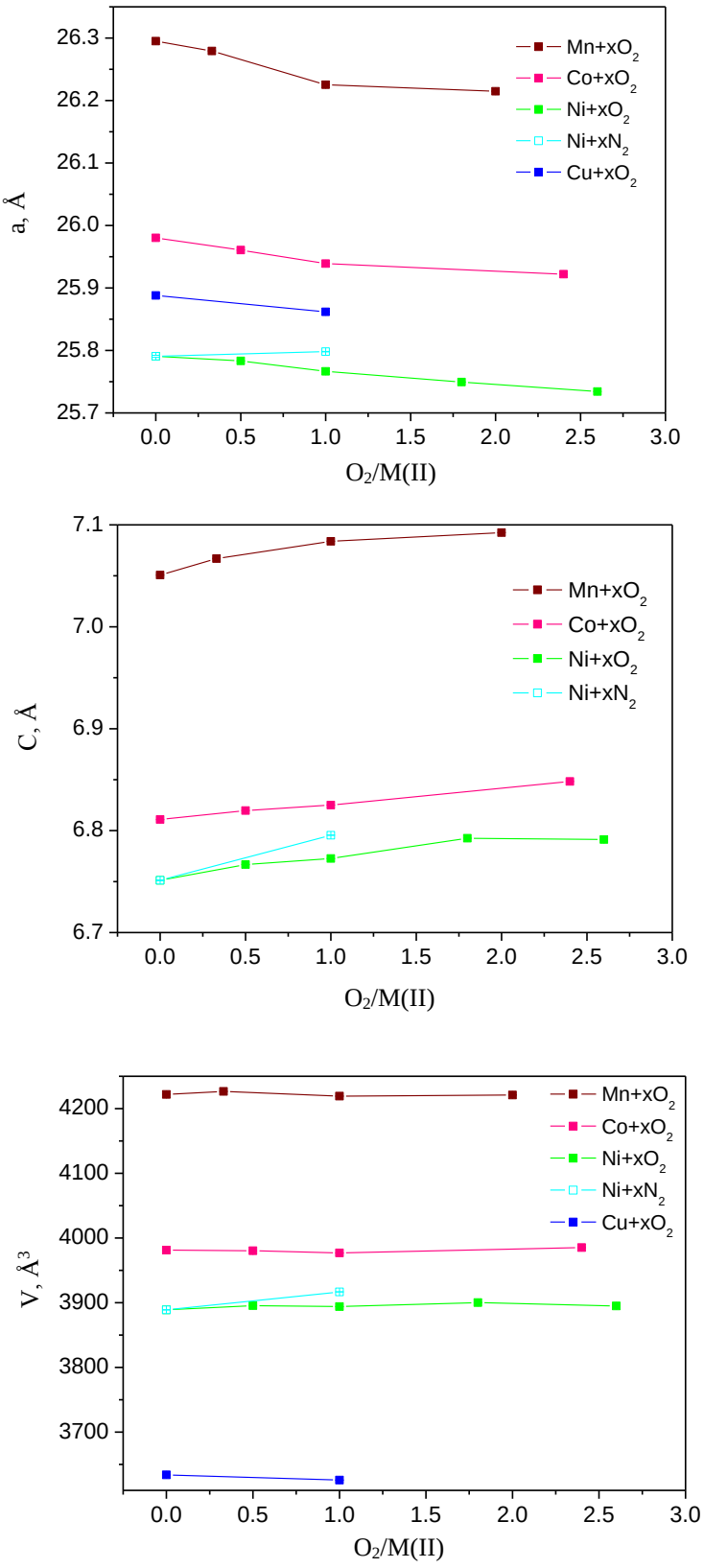

Figure S73. Lattice parameter **a** (top), **c** (middle), and cell volume (bottom) of CPO-27-M(II) in dependence of O_2 loading obtained from the low temperature neutron diffraction data. The **c** lattice parameter of CPO-27-Cu is practically constant at approx.. 6.2 Å, much outside the useful range of the corresponding figure, and is omitted to preserve the y-axis scaling.